Long term low latitude and high elevation cosmogenic 3 He production rate inferred from a 107 ka-old lava flow in northern Chile; 22°S-3400 m a.s.l.

Romain Delunel, Pierre-Henri Blard, Léo C.P. Martin, Sébastien Nomade, Fritz Schlunegger

Long term low latitude and high elevation cosmogenic ^{3}He production rate inferred from a 107 ka-old lava flow in Northern Chile; 22°S-3400 m a.s.l.

Romain Delunel[1,*], Pierre-Henri Blard[2], Léo C. P. Martin[2], Sébastien Nomade[3] and Fritz Schlunegger[1]

[1] Institute of Geological Sciences, University of Bern, Bern, Switzerland
[2] CRPG, UMR 7358, CNRS, Université de Lorraine, Vandoeuvre-lès-Nancy, France
[3] Laboratoire des Sciences du Climat et de l'Environnement, IPSL, CEA-CNRS-UVSQ et Université Paris-Saclay, Gif-sur-Yvette, France

* Corresponding author: Romain Delunel (romain.delunel@geo.unibe.ch; Tel: 0041316318773)

P.-H. Blard, blard@crpg.cnrs-nancy.fr
L.C.P. Martin, leom@crpg.cnrs-nancy.fr
S. Nomade, sebastien.nomade@lsce.ipsl.fr
F. Schlunegger, fritz.schlunegger@geo.unibe.ch

Manuscript revised for submission to Geochimica et Cosmochimica Acta, April 2016

6 Tables, 6 Figures, 2 files as supplementary materials, 72 references
Main text: 6354 words. Abstract: 276 words.

Abstract

Available geological calibration sites used to estimate the rate at which cosmogenic ^{3}He is produced at the Earth's surface are mostly clustered in medium to high latitudes. Moreover, most of them have exposure histories shorter than tens of thousands of years. This lack of sites prevents a qualitative assessment of available production models used to convert cosmogenic ^{3}He concentrations into exposure ages and/or denudation rates. It thus limits our ability to take into account the atmospheric, geomagnetic and solar modulation conditions that might have affected the production of cosmogenic nuclides in the past for longer exposure histories and in low latitude regions. We present the cosmogenic ^{3}He production rate inferred from a new geological calibration site located in northern Chile. Five samples were collected on the surface of the largest and best-preserved lava flow of the San Pedro volcano (21.934°S-68.510°W- 3390 m a.s.l), which displays pristine crease-structure features. $^{40}Ar/^{39}Ar$ dating yielded a reliable plateau age of 107±12 ka for the eruption of this lava flow. Eight pyroxene aliquots separated from the surface samples yield a weighted average cosmogenic ^{3}He concentration of 99.3±1.2 $Mat.g^{-1}$ from which a local cosmogenic ^{3}He production rate of 928±101 $at.g^{-1}.yr^{-1}$ is calculated. The local production rate is then scaled to a sea level high latitude (SLHL) reference position using different combinations of geographic spatialization schemes, atmosphere models and geomagnetic field reconstructions, yielding SLHL production rates between 103±11 and 130±14 $at.g^{-1}.yr^{-1}$ consistent with the most recent estimates available from the literature. Finally, we use the same scaling frameworks to re-evaluate the mean global-scale cosmogenic ^{3}He

production rate in olivine and pyroxene minerals at 120±16 at.g^{-1}.yr^{-1} from the compilation of previously published calibration datasets.

1. Introduction

Studies relying on dating landforms and quantifying rates of Earth surface processes have greatly benefitted from the recent development of Terrestrial Cosmogenic Nuclides (TCN; see von Blanckenburg and Willenbring, 2014 and references therein for a review). Since the mid-80s (e.g. Craig and Poreda, 1986; Kurz, 1986), cosmogenic helium-3 (^{3}He) has been successfully used to date geologic features in various environments and over periods of times ranging from hundreds to millions of years (e.g. Kurz et al., 1990; Licciardi et al., 1999; Schäfer et al., 1999; Evenstar et al., 2009). Cosmogenic ^{3}He combines high production rates (> 100 at.g^{-1}.yr^{-1} at sea level and high latitude) and low analytical detection limits (ca. 10^{5} at.g^{-1} in most favorable cases) with the absence of radioactive decay (i.e. ^{3}He is stable). Cosmogenic ^{3}He also has the advantage to be produced and quantitatively retained over geological timescales in mafic minerals such as olivines and pyroxenes, which offers an interesting alternative for applying surface exposure dating in volcanic terrains where quartz-bearing lithologies might not be available for ^{10}Be and ^{26}Al measurements.

The rate at which cosmogenic ^{3}He is produced at the Earth's surface has been estimated between 100 and 140 at.g^{-1}.yr^{-1} (see Dunai, 2010 and reference therein) from several geological calibration datasets with independent age assignments (e.g. Ackert et al., 2003; Amidon and Farley, 2011; Blard et al., 2006; 2013; Cerling and Craig, 1994; Dunai and Wijbrans, 2000; Fenton et al., 2013; 2014, Foeken et al., 2012; Goehring et al., 2010; Licciardi et al., 1999; 2006). At a global scale, cosmogenic ^{3}He production rates at sea level and high latitude

(SLHL) were estimated using the time-dependent adaptation of the Lal (1991)/Stone (2000) scaling scheme ("Lm"; Balco et al., 2008). The available calibration datasets yielded values of 119±9.9 $at.g^{-1}.yr^{-1}$ for pyroxene (Goehring et al., 2010) and 116±13 (Goehring et al., 2010), 122±15 (Blard et al., 2013) and ca. 117 $at.g^{-1}.yr^{-1}$ (Borchers et al., 2016) when ^{3}He concentrations of both pyroxene and olivine minerals are considered. Although the global-scale SLHL cosmogenic ^{3}He production rates are consistent within associated uncertainties, Phillips et al. (2016) recently emphasized that the initial datasets used in these compilations are clustered both in space (medium to high latitudes) and time (ca. 5-20 ka). According to these authors, this circumstance prevents reliable integrations of past atmospheric, geomagnetic and solar modulation conditions that might have affected the production of cosmogenic nuclides at the Earth's surface. In particular, cosmogenic ^{3}He calibration data are lacking at latitudes < 25° (Blard et al., 2013), where large temporal variations in the paleo magnetic-field intensity might have significantly affected the production of cosmogenic nuclides (e.g. Dunai and Lifton, 2014). Accordingly, improving the accuracy of time dependent corrections requires more low latitude calibration sites with exposure durations significantly longer than 20 ka.

This article presents a new calibration of the cosmogenic ^{3}He production rate from a site located in the hyperarid region of Northern Chile (3400 m a.s.l., ca. 22°S), over a long exposure time (ca. 107 ka). The aim is to reduce the lack of long exposure calibration sites located at high elevation/low latitude. Five samples were collected for helium analyses on top of an andesitic lava flow. This surface is characterized by pristine crease-structure features, which are common on silicic volcanic flows and previously identified as reliable targets for surface

exposure dating (Anderson et al., 1994). First we document the age of a lava flow of the San Pedro volcano using $^{40}Ar/^{39}Ar$ dating techniques. We then report the results of the cosmogenic ^{3}He measurements from five samples (8 aliquots) from which we infer the local production rate of cosmogenic ^{3}He, as well as the production normalized to sea level and high latitude (SLHL), both integrated over the age of the lava flow. Finally, we combine our results with previously reported cosmogenic ^{3}He calibration datasets, based on which we re-evaluate the global ^{3}He production rate at SLHL.

2. Geological setting and sampling

2.1. Volcanic architecture

The San Pedro volcano (6159 m a.s.l., Figure 1) is situated in the El Loa province of Northern Chile ca. 80 km north east of Calama and 100 km north of San Pedro de Atacama. While the San Pedro volcano is located on the western slope of the High Andean Cordillera and therefore does not belong to the Atacama Desert *stricto sensu*, it is characterized by a hyperarid climate, with annual precipitation < 100 mm/y (Houston and Hartley, 2003). The San Pedro volcano is paired with the San Pablo volcano (6118 m a.s.l.) located 5 km further to the east. It represents one of the highest and best-preserved volcanic edifices of the Central Volcanic Zone (de Silva and Francis, 1991), one of the four active volcanic zones in the Andes (see Hora et al., 2007 and reference therein). Only few studies (Francis et al., 1974; Thorpe et al., 1976 and O'Callaghan and Francis 1986) described and identified the nature and composition of erupted materials and the history of eruption of these volcanoes. The San Pedro volcano represents a

104 composite andesitic stratovolcano (Figure 2) made of two east-west oriented
105 coalescent cones that have been successively built as the volcanic belt shifted
106 westward (O'Callaghan and Francis, 1986). The cones stand >2 km above an
107 extensive ignimbrite plateau (Figure 1) that has formed since the Late Miocene
108 at ca. 10.4 Ma during the development of the Altiplano-Puna volcanic complex
109 (de Silva, 1989). The San Pedro cones have been built due to the eruption of
110 silicic materials ranging from basaltic andesite to potassium-rich dacite
111 (O'Callaghan and Francis, 1986). Structural mapping and petrologic
112 investigations (Francis et al., 1974; O'Callaghan and Francis, 1986) revealed that
113 the San Pedro Volcano records three evolutionary steps, comprising i) the
114 edification and subsequent collapse of an "old cone", whose summit marks the
115 highest peak of the volcano, ii) the construction, c.a. 5 km to the west, of the
116 "young cone" that has produced several large lava flows and is still marked by
117 fumarolic activity and iii) the formation of the South West Dome and La Poruña
118 scoria cone, representing the last eruptive episode and associated with the
119 emission of two large and well preserved lava flows (Figure 1). Above 4500 m
120 a.s.l., Francis et al. (1974) reported the presence of glacial moraines and cirques
121 on the southern flanks of both the San Pablo and San Pedro volcanoes. Thus, the
122 last eruptions are probably older than the last large glacial advances in the
123 region (i.e. ca. > 15 ka; Blard et al., 2013). In addition, Wörner et al. (2000)
124 reported an exposure age of ca. 103 ka based on the cosmogenic-^{3}He analysis of
125 one sample collected on La Poruña (Figure1), suggesting that the lava flow
126 emitted by the SW Dome might be at least 100 ka old, or even older.
127
128 *2.2. The SW Dome of the San Pedro volcano*

129 The lava flow emitted by the SW Dome is the largest of the San Pedro volcano. It
130 extends towards the south west for ca. 13 km from ca. 4800 m to 3370 m a.s.l
131 (Figure 1) and covers an area of ca. 20 km^2 with a volume estimated at 2.8 km^3
132 (O'Callaghan and Francis, 1986). The lava flow is considered the product of a
133 200-m-thick early pyroxene dacite lava flow that was locally overlain by
134 subsequent hornblende dacite flows (Figure 1). Although most of the surface of
135 the lava flow displays a rough blocky structure typical of low-viscosity Andean
136 andesite/dacite flows, its distal part presents smooth stream-oriented and
137 elongated features (Figure 2). These features correspond to crease structures
138 (Anderson and Fink, 1992) as inferred from the curved and striated walls
139 situated on both sides of a main central fracture (Figure 2). Such crease
140 structures have been identified as typical constructional volcanic features
141 materializing excellent landforms for surface exposure dating with in-situ
142 produced cosmogenic nuclides (Anderson et al., 1994).
143
144 *2.3. Sampling site*
145 Samples were collected on the top of one crease structure immediately above the
146 main lava flow front. The site is characterized by a perfectly preserved rind crust
147 displaying stream-parallel striations (Table 1, Figures 1 and 2). We collected 5
148 different samples at a few meters interval in order to capture variations in noble
149 gas concentrations that might be related with differences in the preservation of
150 the flow surface. All sampled surfaces showed no sign of post-eruptive erosion or
151 burial. Seasonal snow cover is unlikely given the hyperaridity of the local climate.
152 Samples were collected with a combination of drill-hammer, sledge-hammer and
153 chisels in order to extract homogeneous <10-cm-thick rock cuboids. Samples'

154 locations were recorded with a hand-GPS, and both the local surface geometry
155 and its surrounding topography were measured with a sighting compass and
156 inclinometer. These measurements were later used to correct for geomorphic
157 shielding using equations from Dunne et al. (1999).
158
159 **3. Experimental procedures**
160
161 The following sections provide a description of the sample preparation and
162 analytical experiments conducted for the determination of the eruption age of
163 the San Pedro volcano lava flow via $^{40}Ar/^{39}Ar$ dating and the quantification of the
164 cosmogenic ^{3}He concentrations of the collected samples.
165
166 *3.1 Sample preparation*
167 Before proceeding to the preparation of samples for $^{40}Ar/^{39}Ar$ dating and helium
168 analyses, the rocks were sawed and 3 separates of each sample were used for
169 estimating the lava density. In addition, the bulk rock composition of major
170 elements was measured on one additional sample separate (Table 1, Table 2).
171 Each sample's average density was determined by weighing several times the
172 sample fragments in air and immersed. Bulk rock composition of collected
173 samples was obtained from mass-spectrometry analyses conducted by
174 Activation Laboratories Ltd. (Canada).
175 After measuring the sample thickness, materials for $^{40}Ar/^{39}Ar$ and helium
176 analyses were crushed via electrodynamic disaggregation using the high-voltage
177 pulsed power selFrag-Lab instrument at the Institute of Geological Sciences of
178 the University of Bern. This crushing equipment was preferred to a usual jaw

crusher because of its efficiency in liberating mono-mineral phenocrysts. It also results in a lower loss of material due to mechanical fining, thereby increasing the recovery of mineral separates. Moreover, it has been shown that the electrodynamic disaggregation of rocks do not affect the noble gas content of liberated minerals (Giese et al., 2009). After crushing, the samples were sieved. The 65-125 microns fraction of the sample SP12-02A was processed in order to extract the potassium-rich groundmass for $^{40}Ar/^{39}Ar$ dating purposes. Mafic minerals such as pyroxene, amphibole and associated oxides where first removed using a magnetic separator, after which the remaining material was leached in 10% HNO_3 and rinsed several times with deionized water before small aggregates of clean groundmass were hand-picked under a binocular microscope. About 150 mg were finally used for the $^{49}Ar/^{39}Ar$ dating.

Sample preparation for helium analyses consisted of the separation of heavy minerals from the 250-500 microns fraction using bromoform ($CHBr_3$, 2.9 $g.cm^{-3}$) and methylene iodide (CH_2I_2, 3.3 $g.cm^{-3}$) heavy liquids. Pure separates of pyroxenes without any adhering lava or solid-inclusions were carefully handpicked under a binocular microscope. Clinopyroxene (augite, prismatic greenish grains) and orthopyroxene (enstatite, orthorhombic brownish grains) were isolated. We used color and shape as criteria for mineral separation during picking. Mineral separates were then sonicated with acetone and rinsed several times with deionized water. About 15 grains of each separate were mounted on epoxy-resin discs in order to measure the equivalent spherical radius of the phenocrysts and to determine the composition in major elements of the mineral separates. This was accomplished using the electron microprobe (JEOL-8200) of the Institute of Geological Sciences in Bern. Laser ablation (LA) ICP-MS analyses

were subsequently conducted at the University of Bern on the two discs of sample SP12-02D (i.e. both the clino- and orthopyroxene separates) in order to measure the concentration of a selection of trace elements, notably U, Th, Sm, Li and Gd (Table 3). These data were later used for correcting the helium analyses for the inherited nucleogenic and radiogenic components.

3.2. $^{40}Ar/^{39}Ar$ analytical method

About 150 mg of groundmass from SP12-02A was irradiated for 1 hour (IRR-95) in the OSIRIS nuclear reactor (β1 tube, CEA Saclay, France). After irradiation, ca. 40 mg of the sample was transferred into a stainless steel sample holder and then loaded into a differential vacuum Cleartran® window. Argon isotopes were then extracted from the groundmass by step heating using a 25 W CO_2 laser (Synrad®). Ar isotopes were analyzed using a VG5400 mass spectrometer equipped with a single ion counter following the protocol reported in Nomade et al. (2010). Each Ar isotope measurement consisted of 20 cycles of peak jumping over the argon isotopes. Neutron fluence (J) was monitored by co-irradiation of Alder Creek Sanidine (ACs-2, Nomade et al., 2005) placed in the same pit as the sample. J values were determined from analyses of three ACs-2 single grains. Corresponding J value was calculated using an age of 1.194 Ma (Nomade et al., 2005) and the total decay constant reported by Steiger and Jäger (1977). An $^{40}Ar/^{36}Ar$ atmospheric ratio of 298.56 was then applied (Lee et al., 2006), consistent with the value reported by Valkiers et al., (2010). Recent revisions of decay and monitor constants suggest values about 0.64 % (Kuiper et al., 2008, 1.201 Ma for ACs-2) and 1.0 % (Renne et al., 2011; 1.2059 Ma for ACs-2) older than used here. However, the implied difference in calibrated age is negligible for

our samples (ca. 1 ka) and therefore remains identical within uncertainty with the age reported here. Procedural blanks were measured every three to four steps depending on the beam size. For a typical 10-minutes static blank, typical backgrounds were about (2-5) × 10^{-17} and (4-5) × 10^{-19} moles for ^{40}Ar and ^{36}Ar, respectively. The precision and accuracy of the mass discrimination correction was monitored by daily measurements of air argon at various pressures (Nomade et al., 2010). Nucleogenic production ratios used to correct for reactor produced Ar isotopes from K and Ca could be found in the full data table (Table A1). Data reductions were done using ArArCalc (Koppers, 2002). Plateau age and corresponding uncertainty were calculated using IsoPlot 3.0 (Ludwig, 2003).

3.3. Helium analyses

Helium analyses were carried out at the CRPG noble-gas lab in Nancy, France. ^{3}He and ^{4}He isotope concentrations were measured using the Split Flight Tube mass spectrometer designed by GV. The magmatic contribution to the measured ^{3}He and ^{4}He concentrations was estimated by a 6 min in-vacuo crushing (Kurz, 1986; Scarsi, 2000) of 97 mg of an aliquot of orthopyroxene of sample SP12-02D. These values were then used for all other samples, assuming that the magmatic contribution is the same in all pyroxenes collected on the San Pedro lava flow. Following Williams et al. (2005) and Blard et al. (2013), we also considered that a potential magmatic contribution is negligible in these micro-phenocrysts.

Between ca. 12 and 28 mg of clino- and orthopyroxene were packed in tin foils and fused in-vacuo for 15 min at 1400°C, within an in-house-built single vacuum furnace (Zimmermann et al., 2012). The extracted gas was purified using a succession of activated-charcoal cold traps, Ti-foam and SAES getters. Cryo-

254 focusing of the gas at various temperatures (12 K and 70 K) thus allowed
255 suppression of neon before helium analysis. Following the purification steps, the
256 total ^{3}He and ^{4}He concentrations were analyzed with the SFT mass spectrometer.
257 Re-extraction procedure were conducted on 3 aliquots by heating the furnace to
258 1400°C for an additional 15 min to ensure a complete degasing of the samples.
259 Blank signatures were systematically obtained for these tests. Typical furnace
260 blanks were $(3.3\pm1.1)\times10^{4}$ and $(1.8\pm0.4)\times10^{9}$ atoms for ^{3}He and ^{4}He,
261 respectively, which represent <3% of the total ^{3}He concentrations and ca. 50-
262 80% of the total ^{4}He measured. We emphasize that such a large contribution by
263 the furnace blank to the total ^{4}He signal of the samples is actually not related to
264 the quality of the blanks (i.e. blank values obtained during the experiments were
265 consistent with long term blank values) but rather to the very low ^{4}He content of
266 the samples. The SFT sensitivity was calibrated using a known amount of helium
267 gas standard with a $^{3}He/^{4}He$ ratio of 20.63 Ra ($1Ra=1.384\times10^{-6}$ corresponds to
268 the atmospheric ratio) (Matsuda et al., 2002). The reproducibility at the 1-sigma
269 level on the gas standard was 1.5% for ^{3}He and 0.3% for ^{4}He over a 2-month-
270 period overlapping with our analyses (1 week).
271 Potential contributions in radiogenic ^{4}He due to U, Th and Sm decay were
272 estimated following Blard and Farley (2008). The contribution due to
273 nucleogenic ^{3}He was calculated following Andrews (1985), Andrews and Kay
274 (1982) and using 1) Li concentrations measured in both clino- and
275 orthopyroxene separates of SP12-02D, 2) the compositions in major and trace
276 elements measured in bulk rocks as well as 3) the eruption age of the lava
277 inferred from the $^{40}Ar/^{39}Ar$ dating (Table 2, Table 3, Table 4). The concentration
278 of cosmogenic ^{3}He in our samples ($^{3}He_{c}$) was finally determined using the

equations reported by Kurz (1986) assuming a negligible contribution from radiogenic ^{4}He (Blard and Farley, 2008):

$$^3He_c = {}^3He_t - {}^3He_n - {}^3He_m \quad (1)$$

where ^3He_t is the quantity of ^{3}He measured when fusing the sample, ^3He_n is the nucleogenic component predicted from geochemical analyses of the minerals and bulk rock and ^3He_m the magmatic contribution measured from the in-vacuo crushing of an aliquot of the sample. Note that we do consider here ^3He_c as the product of both spallogenic (induced by high-energy neutrons) and capture reactions (induced by cosmogenic thermal neutrons, CTN). Previous studies reported by e.g. Dunai et al. (2007) and Amidon and Farley (2011) have shown that the contribution of CTN to the cosmogenic ^{3}He concentration depends on the Li concentration of the analyzed minerals and the thermal neutrons flux that irradiates the considered surface. We emphasize, however, that the CTN contribution to the San Pedro samples is likely negligible due to the limited content in Li (<30 ppm) in both the bulk rocks and pyroxene separates (Table 3) and because of the extreme local climate aridity that strongly reduces the probability of H-rich material (e.g. snow) covering the sampled surfaces, and consequently the thermal neutrons flux (see Dunai et al., 2007). We thus anticipate a CTN contribution lower than 5% to the cosmogenic ^{3}He concentrations inferred for the San Pedro samples based on observations reported by Amidon et al. (2009) and Blard et al. (2013b).

4. Results

4.1. ^{40}Ar/^{39}Ar dating of the eruption of the San Pedro Lava flow

The eruption age of the San Pedro volcano lava flow has been estimated from the $^{40}Ar/^{39}Ar$ analyses. Results are presented in table 4 and figure 3. The step-heating degasing spectrum yielded a statistically robust plateau age of 107±12 ka (1σ, Mean Square Weighted Deviates, MSWD=0.07) with 100% of the released ^{39}Ar and no rejected heating steps. The age obtained for the total fusion step is consistent with the plateau age at 109±13 ka (Table 4). Alternatively, Ar data were also cast as inverse isochron age. However, this age is poorly constrained at 100±52 ka, mainly because of the low radiogenic content in the sample resulting in a very limited spread on the isochron. We therefore discarded this age when calculating the production rates of cosmogenic ^{3}He. Instead, we applied the $^{40}Ar/^{39}Ar$ plateau age of 107±12 ka for the calibration of the cosmogenic ^{3}He production rate, as this age yields a good reproducibility at all heating steps. This age is also consistent with the exposure age ca. 103 ka reported by Wörner et al. (2002) for the eruption of La Poruña.

4.2. Helium isotopic results and corrections applied to ^{3}He.

Helium isotope analyses are reported in Table 5 and cosmogenic ^{3}He concentrations ($^{3}He_c$) calculated for the San Pedro volcano samples are plotted in Figure 4. Note that helium concentrations are reported in "Mat.g^{-1}" (i.e. 10^6 atoms per gram of pyroxene or ca. 3.7×10^{-14} cc STP/g) in the following sections. Total concentrations released by melting ranged between 89±3 and 97±3 Mat.g^{-1} for ^{3}He ($^{3}He_t$) and between 29±14 and 90±16 $\times 10^3$ Mat.g^{-1} for ^{4}He ($^{4}He_t$). ^{3}He concentrations cluster around ca. 94±2 Mat.g^{-1}, while the ^{4}He data show a large scatter, which is probably due to the low amount of released gas and the significant contribution of the furnace blank correction (Table 5). In-vacuo

crushing of the aliquot of sample SP12-02D yielded concentrations of (0.29±0.09) Mat.g^{-1} and (17.0±0.6) × 10^3 Mat.g^{-1} for ^{3}He and ^{4}He, respectively (Table 5). The gas liberated during crushing has thus a ^{3}He/^{4}He isotopic ratio of 12±4 Ra that is higher than the values usually reported for volcanic rocks in the Central Andes (Hilton et al., 1993; Blard et al., 2013). This result suggests that unquantifiable amounts of cosmogenic ^{3}He might have been released during in-vacuo crushing, with the consequence that the magmatic correction applied to the samples must be considered as a maximum. However, the impact of this magmatic correction is most likely negligible because the ^{3}He released during crushing (^3He_m) only represents ca. 0.3% of the total ^{3}He released during melting (^3He_t, Table 5). Note that the magmatic ^{3}He correction applied to all the samples was realized using the ^{3}He concentration measured from the prolonged in-vacuo crushing experiment of the sample SP12-02D. This correction systematically represented less than 0.4% of the total ^{3}He extracted by fusion in all samples and thus does not induce a significant source of uncertainty.

Regarding ^{4}He, the concentration we measured during the crushing experiment (17 ± 0.6) ×10^3 Mat.g^{-1} represents ca. 20% of ^4He_t determined in the orthopyroxene aliquot of SP12-02D (77±23) × 10^3 Mat.g^{-1} (Table 5). If we consider that this ^{4}He concentration measured during crushing is magmatic and representative for all samples, then 40 to 80% of ^4He_t is most likely radiogenic in other samples. Using the radiogenic production rates estimated from the minerals composition (P_{4r}: ca. 1.1±0.1 Mat.g^{-1}.yr^{-1}, Table 3), the calculated (U-Th-Sm)/^{4}He ages vary from 12 to 54 ka, i.e. significantly younger than the ^{40}Ar/^{39}Ar age of 107±12 ka. Assuming no magmatic ^{4}He correction, these (U-Th-Sm)/^{4}He ages range from 26 to 76 ka. Such a difference with the ^{40}Ar/^{39}Ar age may

354 indicate that the U, Th and Sm decay chains are out of secular equilibrium (Farley
355 et al., 2002). In any case, given the large uncertainties related to the
356 measurement of ^{4}He concentrations and to the production rate, the (U-Th-
357 Sm)/^{4}He approach cannot be used to thoroughly constrain the age of the flow
358 eruption. We will therefore rely on the $^{40}Ar/^{39}Ar$ age only to calibrate the
359 cosmogenic ^{3}He production rate at the San Pedro volcano.
360 The nucleogenic ^{3}He ($^{3}He_n$) production rates range between ca. 0.1 and 0.2 at.g^{-1}.yr^{-1} (Table 5). The Li concentrations used for this calculation are 20 ppm Li for
362 clinopyroxene and 15 ppm Li for orthopyroxene (from LA ICP-MS analyses of
363 sample SP12-02D, Table 3). Although these values have been used for all 5
364 samples, we emphasize that this simplification does not induce significant
365 uncertainties on the nucleogenic ^{3}He correction as $^{3}He_n$ represents indeed less
366 than 0.03% of $^{3}He_t$ (Table 5).
367
368 *4.3. Calculation of cosmogenic ^{3}He concentrations*
369 Cosmogenic ^{3}He ($^{3}He_c$) reported in Table 5 are corrected for inherited magmatic
370 and nucleogenic components. They range between 89±3 and 96±3 Mat.g^{-1}.
371 Subsequent corrections for thickness, geomorphic shielding and normalization
372 to a geographic position of 21.934°S-68.510°W-3390 m a.s.l. (i.e. total relative
373 correction of ca. 4.5-8.7 %, see Table 1) yield surface cosmogenic ^{3}He
374 concentrations ($^{3}He_{c(S)}$) that range from 93±3 to 102±3 Mat.g^{-1}, with an
375 arithmetic mean of 99±3 Mat.g^{-1}.
376 The $^{3}He_{c(S)}$ concentrations obtained for clinopyroxene and orthopyroxene
377 separates are similar within uncertainties. This is consistent with results from
378 elemental production models (e.g. Masarik and Reedy, 1996) that do not predict

any significant differences in production rate between these two pyroxene phases. Weighted average values can therefore be calculated from clino- and orthopyroxene for the same samples. The narrow distribution displayed by the data thus suggests that all sampled surfaces have experienced the same exposure history. This indicates that the surface of the San Pedro lava flow has not been affected by post-eruptive erosion or burial, consistent with our observations in the field. This also implies that the San Pedro site is suitable for calibrating the production rate of cosmogenic ^{3}He. In summary, the five samples finally yield a weighted average of 99.3±1.2 $Mat_{(3He)}.g_{(pyroxene)}^{-1}$ with a relative standard deviation of ca. 1% and a MSWD of 1.2 (Figure 4).

5. Discussion

5.1. Estimations of cosmogenic ^{3}He production rates

The production rate of cosmogenic ^{3}He can be estimated locally, at the geographic position of the calibration site, and/or scaled to a sea level high latitude (SLHL) reference position. Locally, the cosmogenic ^{3}He production rate is obtained by dividing the average cosmogenic ^{3}He concentration obtained for the calibration site by the age of the considered landform deduced from an independent dating technique (e.g. ^{14}C, K/Ar, ^{40}Ar/^{39}Ar). Note that individual concentrations are first normalized to the surface, an open-sky topography and the mean geographic coordinates (latitude, longitude and elevation) in order to identify potential outliers due to erosion or inheritance (see e.g. Martin et al., 2015, and reference therein). Scaling the cosmogenic ^{3}He production rate to SLHL (referred to as SLHL P3 in following sections) is, however, not

straightforward. The scaling procedure indeed requires the combination of a geographic spatialization model with an atmosphere model and the reconstruction of the past geomagnetic field conditions (see Balco et al., 2008; Lifton et al., 2014). Here we followed a calculation procedure based on a least-square minimization technique (see Martin et al., 2015, for details) and the scaling frameworks presented bellow. SLHL P3 estimates were inferred from the San Pedro samples using the time-independent Lal/Stone scaling model (Lal, 1991; Stone, 2000), noted "St", as well as two time-dependent schemes: "Lm", the adaptation of the Lal/Stone model (Balco et al., 2008) and "LSD", recently developed by Lifton et al. (2014). SLHL P3 estimates were thus obtained by dividing the local production rate by a scaling factor representative for a given combination of scaling, atmosphere and geomagnetic reconstruction models. Regarding scaling schemes, we favored the "Lm" and "LSD" time-dependent models. Indeed, recent studies (Lifton et al., 2014; Borchers et al., 2016; Phillips et al., 2016) have demonstrated that these scaling schemes yield more consistent and reliable spatial and temporal estimates of cosmogenic nuclide production rates than former neutron-monitor based models (Desilets and Zreda, 2003; Desilets et al., 2006; Dunai, 2001; Lifton et al., 2005). These "Lm" and "LSD" models thus represent the most widely used and recently available scaling schemes, respectively (see e.g. Lifton et al., 2014 and Martin et al., 2015). We then calculated SLHL P3s for "St", "Lm" and "LSD" using the Standard atmosphere model (National Oceanic and Atmospheric Administration, 1976) and the ERA-40 reanalysis dataset (Uppala et al., 2005), which allows accounting for the regional variations in height-pressure relationship. Finally, we inferred SLHL P3s for the time-dependent "Lm" and "LSD" scaling schemes with three

paleomagnetic-field reconstruction models (see details regarding the geomagnetic field reconstructions in Martin et al., 2015). The first two geomagnetic models rely on Virtual Dipole Moment values based on 1) Muscheler et al. (2005) for 0-62 ka BP and SINT-2000 (Valet et al., 2005) beyond and 2) GLOPIS-75 (Laj et al., 2004) for 0-75 ka BP and SINT-2000 beyond. The third model is based on the composite reconstruction of temporal variations in geomagnetic and solar intensity modulations implemented in the LSD model (Lifton et al., 2014).

5.2. Calibration of $^{3}He_{c}$ production rates at 21.934°S-68.510°W-3390 m a.s.l.

The local cosmogenic ^{3}He production rate, estimated for the San Pedro calibration site at a geographic position of 21.934°S-68.510°W and 3390 m a.s.l., is obtained by dividing the weighted average $^{3}He_{c(s)}$ with the eruption age of the San Pedro lava flow obtained from the $^{40}Ar/^{39}Ar$ dating. This approach yields a local production rate of 928±11 at.g^{-1}.yr^{-1}, and 928±101 at.g^{-1}.yr^{-1} when propagating both the cosmogenic ^{3}He and $^{40}Ar/^{39}Ar$ uncertainties respectively, at the 1-sigma level (Table 5). This rate combines all production pathways of cosmogenic ^{3}He including spallation, thermal neutron capture and muogenic production. We note however, that the contribution of cosmogenic thermal neutrons to the production of cosmogenic ^{3}He at the San Pedro calibration site is likely lower than 5% and therefore negligible, based on the predictions obtained with the model reported by Amidon and Farley (2011) for pyroxenes with 15-20 ppm apparent Li and a He-closure age of ca. 100 ka.

The local cosmogenic ^{3}He production rate is then scaled to a sea level and high latitude (SLHL) reference position. SLHL P3s inferred from the San Pedro

samples are presented in Table 6. SLHL P3s obtained from the time-independent "St" scheme with the Standard and ERA-40 atmosphere models are 132±14 and 143±16 at.g^{-1}.yr^{-1}, respectively. SLHL P3s estimated with the time-dependent "Lm" and "LSD" schemes, with various combinations of atmosphere and geomagnetic models, vary from 103±11 to 130±14 at.g^{-1}.yr^{-1} (Table 6). In general, the inferred values agree well with the SLHL P3 reported from global-scale compilations by Goehring et al. (2010) and more recently by Blard et al. (2013a). Moreover, SLHL P3s that we estimated using the time-dependent adaptation of the Lal/Stone scaling scheme ("Lm") with the Muscheler-SINT2000 geomagnetic reconstruction and considering both the Standard and ERA-40 atmosphere models are 120±13 and 130±14 at.g^{-1}.yr^{-1}, respectively. Interestingly, these SLHL P3 estimates fit perfectly with the values reported by Blard et al. (2013a) from a ca. 15-ka-old calibration site located at 3800 m a.s.l. on the Bolivian Altiplano (Figure 1).

Note that all applied time-dependent scaling frameworks predict that at the San Pedro volcano calibration site, the production of cosmogenic nuclides, including cosmogenic ^{3}He, has been generally higher during the last 100 to 150 ka than at present (Figure 5). Such a situation can be explained by the persistence of a weaker geomagnetic field intensity that has induced lower cutoff rigidities, thereby allowing more cosmic-ray particles to enter the Earth's magnetic field (see Dunai and Lifton, 2015 and references therein). This effect is particularly amplified in high tropical areas integrating >50-ka exposure histories (e.g. Balco et al., 2008), since it yields relative corrections between 10 and 20% of the modern rate (Figure 5). It thus explains why the San Pedro calibration site yields time-independent "St" scaling factors that are higher than those inferred from

479 time-dependent schemes ("Lm" and "LSD"). Figure 5 and Table 6 illustrate that
480 geomagnetic field reconstructions relying on the Muscheler-SINT2000 and "LSD"
481 frameworks systematically yield the highest and lowest SLHL P3s, respectively,
482 independently of the scaling scheme and atmosphere model considered. The
483 geomagnetic field and solar modulation reconstructions implemented in the
484 "LSD" frameworks predict time-integrated scaling factors that are up to ca. 10%
485 higher than with the Muscheler-SINT2000 for an exposure length > 60 ka.
486
487 *5.3. Re-evaluation of the global SLHL cosmogenic ^{3}He production rate*
488 Cosmogenic ^{3}He production rates have rarely been calibrated to sea level high
489 latitude positions using a common calculation framework that included similar
490 scaling schemes, atmosphere model and geomagnetic field reconstructions. Here
491 we re-evaluate the global SLHL P3 by compiling and processing available
492 calibration datasets for both olivine and pyroxene within a common calculation
493 framework that combines the scaling schemes, atmosphere and geomagnetic
494 field models presented above (see section 3.4). Twenty different calibration sites
495 and ca. 150 cosmogenic ^{3}He analyses have been compiled from the literature and
496 combined with the San Pedro samples (see Table A2). This new compilation
497 includes the studies of Ackert et al. (2003), Amidon and Farley (2011), Blard et
498 al. (2006, 2013a), Cerling and Craig (1994); Dunai and Wijbrans (2000), Fenton
499 et al. (2013, 2014), Foeken et al. (2012), Goehring et al. (2010) and Licciardi et al.
500 (1999, 2006). We do note that we only considered dataset originating from
501 absolute calibration studies and therefore excluded those from cross calibrations
502 (e.g. Amidon et al, 2009). Some of the studies included in this compilation did not
503 address the impact of radiogenic ^{4}He on the measured cosmogenic ^{3}He

concentrations. In several of these previous studies indeed, the authors overestimated the amount of ^{4}He that was derived from trapped magmatic gases and thus over-corrected for magmatic ^{3}He, thereby resulting in an underestimation of cosmogenic ^{3}He concentrations. To tackle this issue, the compiled data were first corrected for this radiogenic contribution, either using the reported U-Th-Sm concentrations in the phenocrysts or considering the global mean of these elements as proposed by Blard and Farley (2008, see Table A2). The resulting corrections slightly increase the cosmogenic ^{3}He concentrations by 4% on average, as illustrated in the inset of Figure 6A. Subsequently, the cosmogenic ^{3}He concentrations available for each calibration site were 1) normalized to the surface, an open-sky topography and the sites' mean geographic coordinates, 2) used to calculate a weighted average concentration and 3) inverted to SLHL P3s, following the procedure outlined in section 3.4. SLHL P3s inferred from all possible combinations in scaling, atmosphere and geomagnetic field models cover the range 76±4 – 186±12 $at.g^{-1}.yr^{-1}$ (see Table A2). When considering each scaling framework separately, the values yield arithmetic means that range between 115±19 and 122±20 $at.g^{-1}.yr^{-1}$, therefore identical within uncertainty (1σ-level). These re-evaluated global SLHL P3s are consistent with values reported from previous compilations that also considered olivine and pyroxene minerals together (e.g. Goehring et al., 2010; Blard et al., 2013a; Borchers et al., 2016). We emphasize, however, that SLHL P3s estimated from the combination of the "Lm" scaling scheme with the ERA-40 atmosphere model and the geomagnetic field reconstruction based on Muscheler (2004) and SINT2000 (Valet et al., 2004) yield the least scatter in the distribution, with a 14% relative standard deviation and an arithmetic mean of

120±16 at.g^{-1}.yr^{-1}. Figure 6 represents the distribution of SLHL P3s inferred from this latter scaling framework. It does not show any correlation with elevation nor with latitude. This confirms previous observations reported by Goehring et al. (2010) and Blard et al. (2013a) that there is no anomalous production of cosmogenic ^{3}He at high elevations, at least in pyroxene and olivine. It is, however, important to emphasize that the estimated Mean Square Weighted Deviation is significantly higher than 1 (MSWD = 10.4; Figure 6), indicating that the observed variability in the data is larger than a statistical dispersion that would result from analytical uncertainties only. In other words, the global SLHL P3 compilation unlikely represents a single population. Note that while Figure 6 only represents SLHL P3s estimated from the combination of the "Lm" scaling scheme with the ERA-40 atmosphere model and Muscheler-SINT2000 based geomagnetic field reconstruction, all other scaling frameworks present a similar picture. Part of this over-dispersion might result from calibration sites older than ca. 120 ka that systematically yield SLHL P3s lower than ca. 110 at.g^{-1}.yr^{-1} when considering the "Lm" scaling scheme (Figure 6). This inference, however, should be tuned down when considering the "LSD" scaling scheme, as P3s estimates do not show such temporal pattern. In any cases and for all considered scaling frameworks, the variability in SLHL P3s seems independent from the exposure age for calibration sites younger than 110 ka (Figure 6). The observed variability in SLHL P3s might result from unrecognized erosion, variations in atmospheric pressure, inaccurate correction of the time-dependent production rate variability, and/or unaccounted excess in Li concentrations of crustally contaminated magmas (e.g. Amidon et al., 2011; Dunai and Wijbrans, 2000; Dunai et al., 2007; Foeken et al., 2012; Staiger et al., 2007). Excluding calibration

554 sites older than 120 ka from the global compilation leads to slightly higher
555 average cosmogenic ^{3}He production rates by ca. 2-4% and reduces the standard
556 deviations from 14-17% to ca. 11-17%, depending on the considered scaling
557 framework (see Table A2), but do not fundamentally change the overall picture.
558 In summary, SLHL P3s inferred from the combination of the "Lm" scaling scheme
559 with the ERA-40 atmosphere model and Muscheler-SINT2000 based
560 geomagnetic field reconstruction yield the best constrained mean global-scale
561 cosmogenic ^{3}He production rate. This scaling framework therefore represents a
562 qualitative combination of currently available geographic spatialization schemes,
563 atmosphere as well as geomagnetic field reconstruction models to estimate
564 exposure ages from cosmogenic ^{3}He concentrations. Similar statements were
565 also reported by Martin et al. (2015) regarding the production of in-situ ^{10}Be in
566 the high tropical Andes.
567
568 **6. Conclusion**
569
570 We report a new geological calibration site located in northern Chile (21.934°S-
571 68.510°W) at 3390 m a.s.l. that we used to infer the production rate of
572 cosmogenic ^{3}He in pyroxenes. ^{40}Ar/^{39}Ar dating gives a consistent plateau age of
573 107±12 ka. Eight mineral separates of clino- and orthopyroxene from five
574 different surface samples yield clustered ^{3}He concentrations, for both pyroxene
575 phases. Magmatic and nucleogenic ^{3}He corrections are negligible (< 1%) in this
576 lava flow. The weighted average cosmogenic ^{3}He concentration is 99.3±1.2 Mat.g^{-}
577 ^{1}, which represents the highest cosmogenic ^{3}He concentrations ever measured so
578 far in natural calibration samples.

579 We then used this data to constrain a local cosmogenic ^{3}He production rate of
580 928±101 at.g^{-1}.yr^{-1} at 21.934°S-68.510°W and 3390 m a.s.l. After scaling to sea
581 level and high latitudes (SLHL), cosmogenic ^{3}He production rate estimates vary
582 from 103±11 to 130±14 at.g^{-1}.yr^{-1}, which depends on different combinations of
583 scaling schemes, atmosphere models and geomagnetic field reconstructions.
584 Finally we combined the SLHL P3s inferred from the San Pedro lava flow
585 samples with cosmogenic ^{3}He production rates (in both olivine and pyroxene)
586 inferred from various calibration sites and re-evaluated the mean global SLHL
587 P3. This compilation, where cosmogenic ^{3}He production rates were scaled to
588 SLHL with two scaling schemes, two atmosphere models and three different
589 geomagnetic field reconstructions, yield arithmetic means for SLHL P3s that vary
590 between 115±19 and 122±20 at.g^{-1}.yr^{-1}. These values are identical within
591 uncertainty and consistent with values previously reported from similar
592 compilation studies (e.g. Goehring et al., 2010; Blard et al., 2013a; Borchers et al.,
593 2016). This new compilation thus illustrates that a calculation framework
594 including the (1) time-dependent adaptation of the Lal (1991) / Stone (2000)
595 scheme, (2) ERA-40 atmosphere model (Uppala et al., 2005), and a (3)
596 geomagnetic field reconstruction relying on the Virtual Dipole Moment values
597 based on Muscheler et al. (2004) and SINT-2000 (Valet et al., 2005) currently
598 yields the best constrained mean global-scale cosmogenic ^{3}He production rate.
599 Our observations also appear perfectly in line with the recent findings reported
600 by Lifton (2016). We thus suggest that the update of the scaling framework
601 presented here, together with the inferred mean global SLHL P3 of 120±16 at.g^{-}
602 ^{1}.yr^{-1}, should be favored when calculating exposure ages from cosmogenic ^{3}He
603 concentrations.

Acknowledgments

This project received financial supports by the Swiss National Science Foundation awarded to Schlunegger (grant No. 137516). We thank Christine Lemp, Martin Robyr and Thomas Pettke for their support during sample preparation and geochemical analyses. We thank David L. Shuster for his careful editorial handling, as well as Will Amidon and an anonymous reviewer who provided constructive comments on the submitted manuscript.

References

Ackert, R.P., Singer, B.S., Guillou, H., Kaplan, M.R., Kurz, M.D., 2003. Long-term cosmogenic ^{3}He production rates from ^{40}Ar/^{39}Ar and K–Ar dated Patagonian lava flows at 47°S. *Earth and Planetary Science Letters 210*, 119-136.

Amidon, W.H., Rood, D.H., Farley, K.A., 2009. Cosmogenic ^{3}He and ^{21}Ne production rates calibrated against ^{10}Be in minerals from the Coso volcanic field. *Earth and Planetary Science Letters 280*, 194-204.

Amidon, W.H., Farley, K.A., 2011. Cosmogenic ^{3}He production rates in apatite, zircon and pyroxene inferred from Bonneville flood erosional surfaces. *Quaternary Geochronology 6*, 10-21.

Anderson, S. W., Fink, J. H., 1992. Crease structures: indicators of emplacement rates and surface stress regimes of lava flows. *Geological Society of America Bulletin 104(5)*, 615-625.

Anderson, S. W., Krinsley, D. H., Fink, J. H. 1994. Criteria for recognition of constructional silicic lava flow surfaces. *Earth Surface Processes and Landforms 19(6)*, 531-541.

Andrews, J., 1985. The isotopic composition of radiogenic helium and its use to study groundwater movement in confined aquifers. *Chemical Geology 49*, 339-351.

Andrews, J., Kay, R., 1983. The U contents and ^{234}U/^{238}U activity ratios of dissolved uranium in groundwaters from some Triassic sandstones in England. *Chemical Geology 41*, 101-117.

Balco, G., Stone, J.O., Lifton, N.A., Dunai, T.J., 2008. A complete and easily accessible means of calculating surface exposure ages or erosion rates from ^{10}Be and ^{26}Al measurements. *Quaternary Geochronology 3*, 174-195.

Blard, P.-H., Farley, K., 2008. The influence of radiogenic ^{4}He on cosmogenic ^{3}He determinations in volcanic olivine and pyroxene. *Earth and Planetary Science Letters 276*, 20-29.

Blard, P.-H., Lavé, J., Sylvestre, F., Placzek, C., Claude, C., Galy, V., Condom, T., Tibari, B., 2013a. Cosmogenic ^{3}He production rate in the high tropical Andes (3800 m, 20°S): implications for the local last glacial maximum. *Earth and Planetary Science Letters 377*, 260-275.

Blard, P.-H., Braucher, R., Lavé, J., Bourlès, D., 2013b. Cosmogenic ^{10}Be production rate calibrated against ^{3}He in the high Tropical Andes (3800-4900 m, 20-22° S). Earth and Planetary Science Letters 382, 140-149.

Blard, P.H., Bourlès, D., Lavé, J., Pik, R., 2006. Applications of ancient cosmic-ray exposures: Theory, techniques and limitations. *Quaternary Geochronology 1*, 59-73.

Blard, P.H., Puchol, N., Farley, K.A., 2008. Constraints on the loss of matrix-sited helium during vacuum crushing of mafic phenocrysts. *Geochimica et Cosmochimica Acta 72*, 3788-3803.

Borchers, B., Marrero, S., Balco, G., Caffee, M., Goehring, B., Lifton, N., Nishiizumi, K., Phillips, F., Schaefer, J., Stone, J., 2016. Geological calibration of spallation production rates in the CRONUS-Earth Project. *Quaternary Geochronology 31, 188-198*.

660 Cerling, T.E., Craig, H, 1994. Cosmogenic ^{3}He production rates from 39°N to 46°N
661 latitude, western USA and France. *Geochimica et cosmochimica Acta* 58, 249-
662 255.
663 Craig, H., Poreda, R.J., 1986. Cosmogenic ^{3}He in terrestrial rocks: The summit
664 lavas of Maui. *Proceedings of the National Academy of Sciences 83*, 1970-1974.
665 Desilets, D., Zreda, M., 2003. Spatial and temporal distribution of secondary
666 cosmic-ray nucleon intensities and applications to in situ cosmogenic dating.
667 *Earth and Planetary Science Letters 206*, 21-42.
668 Desilets, D., Zreda, M., Prabu, T., 2006. Extended scaling factors for in situ
669 cosmogenic nuclides: New measurements at low latitude. *Earth and Planetary*
670 *Science Letters 246*, 265-276.
671 De Silva, S., 1989. Altiplano-Puna volcanic complex of the central Andes. *Geology*
672 *17*, 1102-1106.
673 Dunai, T.J., 2001. Influence of secular variation of the geomagnetic field on
674 production rates of in situ produced cosmogenic nuclides. *Earth and Planetary*
675 *Science Letters 193*, 197-212.
676 Dunai, T.J., Stuart, F.M., Pik, R., Burnard, P., Gayer, E., 2007. Production of ^{3}He in
677 crustal rocks by cosmogenic thermal neutrons. *Earth and Planetary Science*
678 *Letters 258*, 228-236.
679 Dunai, T.J., 2010. Cosmogenic nuclides: principles, concepts and applications in
680 the earth surface sciences, New York.
681 Dunai, T.J., Wijbrans, J.R., 2000. Long-term cosmogenic ^{3}He production rates (152
682 ka–1.35 Ma) from ^{40}Ar/^{39}Ar dated basalt flows at 29°N latitude. *Earth and*
683 *Planetary Science Letters 176*, 147-156.
684 Dunai, T.J., Stuart, F.M., Pik, R.l., Burnard, P., Gayer, E., 2007. Production of ^{3}He in
685 crustal rocks by cosmogenic thermal neutrons. *Earth and Planetary Science*
686 *Letters 258*, 228-236.
687 Dunai, T.J., Lifton, N.A., 2014. The nuts and bolts of cosmogenic nuclide
688 production. *Elements 10*, 347-350.
689 Dunne, J., Elmore, D., Muzikar, P., 1999. Scaling factors for the rates of production
690 of cosmogenic nuclides for geometric shielding and attenuation at depth on
691 sloped surfaces. *Geomorphology 27*, 3-11.
692 Evenstar, L.A., Hartley, A.J., Stuart, F.M., Mather, A.E., Rice, C.M., Chong, G., 2009.
693 Multiphase development of the Atacama Planation Surface recorded by
694 cosmogenic ^{3}He exposure ages: Implications for uplift and Cenozoic climate
695 change in western South America. *Geology 37*, 27-30.
696 Farley, K., Kohn, B., Pillans, B., 2002. The effects of secular disequilibrium on (U–
697 Th)/He systematics and dating of Quaternary volcanic zircon and apatite. *Earth*
698 *and Planetary Science Letters 201*, 117-125.
699 Fenton, C.R., Mark, D.F., Barfod, D.N., Niedermann, S., Goethals, M.M., Stuart, F.M.,
700 2013. ^{40}Ar/^{39}Ar dating of the SP and Bar Ten lava flows AZ, USA: Laying the
701 foundation for the SPICE cosmogenic nuclide production-rate calibration
702 project. *Quaternary Geochronology 18*, 158-172.
703 Fenton, C.R., Niedermann, S., 2014. Surface exposure dating of young basalts (1–
704 200 ka) in the San Francisco volcanic field (Arizona, USA) using cosmogenic ^{3}He
705 and ^{21}Ne. *Quaternary Geochronology 19*, 87-105.
706 Foeken, J.P.T., Stuart, F.M., Mark, D.F., 2012. Long-term low latitude cosmogenic
707 ^{3}He production rate determined from a 126 ka basalt from Fogo, Cape Verdes.
708 *Earth and Planetary Science Letters 359–360*, 14-25.

709 Francis, P.W., Roobol, M.J., Walker, G.P.L., Cobbold, P.R., Coward, M., 1974. The
710 San Pedro and San Pablo volcanoes of northern Chile and their hot avalanche
711 deposits. *Geol Rundsch 63*, 357-388.
712 Giese, J., Seward, D., Stuart, F.M., Wüthrich, E., Gnos, E., Kurz, D., Eggenberger, U.,
713 Schreurs, G., 2010. Electrodynamic Disaggregation: Does it Affect Apatite
714 Fission-Track and (U-Th)/He Analyses? *Geostandards and Geoanalytical*
715 *Research 34*, 39-48.
716 Goehring, B.M., Kurz, M.D., Balco, G., Schaefer, J.M., Licciardi, J., Lifton, N., 2010. A
717 reevaluation of in situ cosmogenic ^{3}He production rates. *Quaternary*
718 *Geochronology 5*, 410-418.
719 Hilton, D., Hammerschmidt, K., Teufel, S., Friedrichsen, H., 1993. Helium isotope
720 characteristics of Andean geothermal fluids and lavas. *Earth and Planetary*
721 *Science Letters 120*, 265-282.
722 Hora, J.M., Singer, B.S., Wörner, G., 2007. Volcano evolution and eruptive flux on
723 the thick crust of the Andean Central Volcanic Zone: ^{40}Ar/^{39}Ar constraints from
724 Volcán Parinacota, Chile. *Geol. Soc. Am. Bull. 119*, 343-362.
725 Houston, J., Hartley, A. J., 2003. The central Andean west-slope rainshadow and
726 its potential contribution to the origin of hyper-aridity in the Atacama Desert.
727 *International Journal of Climatology 23(12)*, 1453-1464.
728 Koppers, A.A., 2002. ArArCALC—software for 40 Ar/39 Ar age calculations.
729 *Computers & Geosciences 28*, 605-619.
730 Kuiper, K., Deino, A., Hilgen, F., Krijgsman, W., Renne, P., Wijbrans, J., 2008.
731 Synchronizing rock clocks of Earth history. *Science 320*, 500-504.
732 Kurz, M.D., 1986. In situ production of terrestrial cosmogenic helium and some
733 applications to geochronology. *Geochimica et Cosmochimica Acta 50*, 2855-
734 2862.
735 Kurz, M.D., Colodner, D., Trull, T.W., Moore, R.B., O'Brien, K., 1990. Cosmic ray
736 exposure dating with in situ produced cosmogenic ^{3}He: results from young
737 Hawaiian lava flows. *Earth and Planetary Science Letters 97*, 177-189.
738 Laj, C., Kissel, C., Beer, J., 2004. High Resolution Global Paleointensity Stack Since
739 75 kyr (GLOPIS-75) Calibrated to Absolute Values. *Timescales of the*
740 *Paleomagnetic Field*, 255-265.
741 Lal, D., 1991. Cosmic ray labelling of erosion surfaces: in situ nuclide production
742 rates and erosion models. *Earth and Planetary Science Letters 104*, 424–439.
743 Lee, J.-Y., Marti, K., Severinghaus, J.P., Kawamura, K., Yoo, H.-S., Lee, J.B., Kim, J.S.,
744 2006. A redetermination of the isotopic abundances of atmospheric Ar.
745 *Geochimica et Cosmochimica Acta 70*, 4507-4512.
746 Licciardi, J., Kurz, M., Clark, P., Brook, E., 1999. Calibration of cosmogenic ^{3}He
747 production rates from Holocene lava flows in Oregon, USA, and effects of the
748 Earth's magnetic field. *Earth and Planetary Science Letters 172*, 261-271.
749 Licciardi, J., Kurz, M., Curtice, J., 2006. Cosmogenic 3 He production rates from
750 Holocene lava flows in Iceland. *Earth and Planetary Science Letters 246*, 251-
751 264.
752 Lifton, N.A., Bieber, J.W., Clem, J.M., Duldig, M.L., Evenson, P., Humble, J.E., Pyle, R.,
753 2005. Addressing solar modulation and long-term uncertainties in scaling
754 secondary cosmic rays for in situ cosmogenic nuclide applications. *Earth and*
755 *Planetary Science Letters 239*, 140-161.

Lifton, N., Sato, T., Dunai, T.J., 2014. Scaling in situ cosmogenic nuclide production rates using analytical approximations to atmospheric cosmic-ray fluxes. *Earth and Planetary Science Letters 386*, 149-160.

Lifton, N., 2016. Implications of two Holocene time-dependent geomagnetic models for cosmogenic nuclide production rate scaling. *Earth and Planetary Science Letters 433*, 257-268

Ludwig, K., 2003. User manual for Isoplot 3.0. Berkeley Geochronology Center Special Publication 4.

Masarik, J., Reedy, R., 1996. Monte Carlo simulation of in-situ-produced cosmogenic nuclides. *Radiocarbon 38*, 163–164.

Martin, L.C.P., Blard, P.H., Lavé, J., Braucher, R., Lupker, M., Condom, T., Charreau, J., Mariotti, V., Team, A., Davy, E., 2015. In situ cosmogenic ^{10}Be production rate in the High Tropical Andes. *Quaternary Geochronology 30*, Part A, 54-68.

Matsuda, J., Matsumoto, T., Sumino, K., Nagao, K., Yamamoto, J., Miura, Y., Kaneoka, I., Takahata, N., Sano, Y., 2002. The ^{3}He/^{4}He ratio of the new internal He standard of Japan (HESJ). *Geochemical Journal 36*, 191-195.

Muscheler, R., Beer, J., Kubik, P.W., Synal, H.-A., 2005. Geomagnetic field intensity during the last 60,000 years based on ^{10}Be and ^{36}Cl from the Summit ice cores and ^{14}C. *Quaternary Science Reviews 24*, 1849-1860.

National Oceanic and Atmospheric Administration, 1976. National Aeronautics and Space Administration, and the United States Air Force. Washington, DC

Nomade, S., Renne, P., Vogel, N., Deino, A., Sharp, W., Becker, T., Jaouni, A., Mundil, R., 2005. Alder Creek sanidine (ACs-2): a Quaternary ^{40}Ar/^{39}Ar dating standard tied to the Cobb Mountain geomagnetic event. *Chemical Geology 218*, 315-338.

Nomade, S., Gauthier, A., Guillou, H., Pastre, J.-F., 2010. ^{40}Ar/^{39}Ar temporal framework for the Alleret maar lacustrine sequence (French Massif-Central): Volcanological and paleoclimatic implications. *Quaternary Geochronology 5*, 20-27.

O'Callaghan, L.J., Francis, P.W., 1986. Volcanological and petrological evolution of San Pedro volcano, Provincia EI Loa, North Chile. *Journal of the Geological Society 143*, 275-286.

Phillips, F.M., Argento, D.C., Bourlès, D.L., Caffee, M.W., Dunai, T.J., Goehring, B., Gosse, J.C., Hudson, A.M., Jull, A.T., Kelly, M., 2016. Where now? Reflections on future directions for cosmogenic nuclide research from the CRONUS Projects. *Quaternary Geochronology 31*, 155-159.

Renne, P.R., Balco, G., Ludwig, K.R., Mundil, R., Min, K., 2011. Response to the comment by WH Schwarz et al. on "Joint determination of 40 K decay constants and 40 Ar∗/40 K for the Fish Canyon sanidine standard, and improved accuracy for 40 Ar/39 Ar geochronology" by PR Renne et al. (2010). *Geochimica et Cosmochimica Acta 75*, 5097-5100.

Scarsi, P., 2000. Fractional extraction of helium by crushing of olivine and clinopyroxene phenocrysts: effects on the ^{3}He/^{4}He measured ratio. *Geochimica et Cosmochimica Acta 64*, 3751-3762.

Schäfer, J.M., Ivy-Ochs, S., Wieler, R., Leya, I., Baur, H., Denton, G.H., Schlüchter, C., 1999. Cosmogenic noble gas studies in the oldest landscape on earth: surface exposure ages of the Dry Valleys, Antarctica. *Earth and Planetary Science Letters 167*, 215-226.

803 Staiger, J., Gosse, J., Toracinta, R., Oglesby, B., Fastook, B., Johnson, J.V., 2007.
804 Atmospheric scaling of cosmogenic nuclide production : climate effect. *Journal*
805 *of Geophysical Research 112*, B2, B02205
806 Steiger, R.H., Jäger, E., 1977. Subcommission on geochronology: convention on
807 the use of decay constants in geo-and cosmochronology. *Earth and Planetary*
808 *Science Letters 36*, 359-362.
809 Stone, J.O., 2000. Air pressure and cosmogenic isotope production. *J. Geophys.*
810 *Res.-Solid Earth 105*, 23753-23759.
811 Thorpe, R.S., Potts, P.J., Francis, P.W., 1976. Rare Earth data and petrogenesis of
812 andesite from the North Chilean Andes. *Contr. Mineral. and Petrol. 54*, 65-78.
813 Uppala, S.M., Kållberg, P., Simmons, A., Andrae, U., Bechtold, V., Fiorino, M.,
814 Gibson, J., Haseler, J., Hernandez, A., Kelly, G., 2005. The ERA-40 re-analysis.
815 *Quarterly Journal of the Royal Meteorological Society 131*, 2961-3012.
816 Valet, J.-P., Meynadier, L., Guyodo, Y., 2005. Geomagnetic dipole strength and
817 reversal rate over the past two million years. *Nature 435*, 802-805.
818 Valkiers, S., Vendelbo, D., Berglund, M., De Podesta, M., 2010. Preparation of
819 argon primary measurement standards for the calibration of ion current ratios
820 measured in argon. *International Journal of Mass Spectrometry 291*, 41-47.
821 von Blanckenburg, F., Willenbring, J.K., 2014. Cosmogenic nuclides: Dates and
822 rates of Earth-surface change. *Elements 10*, 341-346.
823 Williams, A.J., Stuart, F.M., Day, S.J., Phillips, W.M., 2005. Using pyroxene
824 microphenocrysts to determine cosmogenic ^{3}He concentrations in old volcanic
825 rocks: an example of landscape development in central Gran Canaria.
826 *Quaternary Science Reviews 24*, 211-222.
827 Wörner, G., Hammerschmidt, K., Henjes-Kunst, F., Lezaun, J., Wilke, H., 2000.
828 Geochronology (^{40}Ar/^{39}Ar, K-Ar and He-exposure ages) of Cenozoic magmatic
829 rocks from Northern Chile (18-22°S): implications for magmatism and tectonic
830 evolution of the central Andes. *Revista geológica de Chile 27*, 205-240.
831 Zimmermann, L., Blard, P.H., Burnard, P., Medynski, S., Pik, R., Puchol, N., 2012. A
832 new single vacuum furnace design for cosmogenic ^{3}He dating. *Geostandards and*
833 *Geoanalytical Research 36*, 121-129.
834

Table 1. Sample characteristics

Sample name	Latitude (°)	Longitude (°)	Elevation (m)	Atmospheric pressure (hPa) [a]	Altitude factor [b]	Sample thickness (cm)	Density ($g.cm^{-3}$)	Thickness correction [c]	Geomorphic shielding [d]	Total correction [e] (%)
SP12-02A	-21.93434	-68.50980	3389	679.55	0.999	6	2.44	0.956	0.996	4.9
SP12-02C	-21.93431	-68.50974	3394	679.13	1.002	6	2.41	0.956	0.995	4.6
SP12-02D	-21.93440	-68.50966	3393	679.22	1.002	6	2.43	0.956	0.998	4.5
SP12-02E	-21.93435	-68.50983	3391	679.38	1.001	7	2.22	0.953	0.998	4.9
SP12-02F	-21.93437	-68.51005	3384	679.97	0.997	7.5	2.21	0.950	0.964	8.7

[a] Local atmospheric pressure was calculated using the ICAO standard atmosphere equation with sea level temperature and pressure derived from the ERA-40 reanalysis dataset (Uppala et al., 2005)

[b] Correction factors used to scale cosmogenic ^{3}He concentrations to 21.934°S-68.510°W, 3390m (679.468 hPa). Values are calculated as the ratio between the scaling factor obtained using the Lal (1991) / Stone (2000) scheme with the ERA-40 atmosphere model for the sampling position and at 21.934°S-68.510°W, 3390 m a.s.l.

[c] Thickness corrections are calculated using an attenuation length of 160 $g.cm^{-2}$ and the sample densities measured.

[d] Total geomorphic shielding, including self-shielding by the sampled surface and the topography around the sampling site, are calculated according to Dunne et al. (1999) and an algorithm provided by G. Balco (http://hess.ess.washington.edu/).

[e] Calculated as the product of altitude, thickness and geomorphic shielding factors.

Table 2. Major element composition of lava and pyroxene phenocrysts

Sample name	Type	SiO_2	Al_2O_3	Fe_2O_3	MnO	MgO	CaO	Na_2O	K_2O	TiO_2	P_2O_5	LOI	Total
		(wt %)	(wt %)	(wt %)	(wt %)	(wt %)	(wt %)	(wt %)	(wt %)	(wt %)	(wt %)	(wt %)	(%)
SP12-02A	Bulk rock	63.3	15.6	5.5	0.08	2.4	4.1	4.0	3.3	0.8	0.2	1.2	100
SP12-02A	Clinopyroxene	52.1	2.4	9.8	-	14.7	19.6	0.5	0.0	0.5	-	-	100
SP12-02A	Orthopyroxene	54.0	0.9	20.0	-	22.9	1.2	0.0	0.0	0.4	-	-	100
SP12-02C	Bulk rock	65.1	14.7	5.4	0.08	2.2	3.9	3.7	3.1	0.8	0.2	1.5	101
SP12-02C	Clinopyroxene	52.7	2.2	8.9	-	14.9	20.4	0.4	0.0	0.4	-	-	100
SP12-02D	Bulk rock	62.8	15.2	5.5	0.08	2.3	4.1	3.7	3.0	0.8	0.2	1.7	99
SP12-02D	Clinopyroxene	52.0	2.4	10.0	-	14.8	19.3	0.5	0.0	0.6	-	-	100
SP12-02D	Orthopyroxene	53.6	1.1	20.5	-	23.1	1.3	0.0	0.0	0.2	-	-	100
SP12-02E	Bulk rock	61.4	15.2	5.4	0.07	2.2	4.6	3.9	3.0	0.8	0.2	2.0	99
SP12-02E	Clinopyroxene	53.0	1.9	8.8	-	14.8	20.3	0.4	0.0	0.4	-	-	100
SP12-02F	Bulk rock	63.8	14.8	5.2	0.08	2.1	4.2	3.7	2.9	0.7	0.2	1.7	99
SP12-02F	Clinopyroxene	52.7	2.0	9.9	-	14.3	20.0	0.5	0.0	0.4	-	-	100
SP12-02F	Orthopyroxene	54.1	0.8	19.4	-	23.4	1.1	0.0	0.0	0.3	-	-	99

Table 3. Trace element composition of lava and pyroxene phenocrysts

Sample name	Type	Li (ppm)	B (ppm)	Cr (ppm)	Co (ppm)	Ni (ppm)	Gd (ppm)	U (ppm)	Th (ppm)	Sm (ppm)
SP12-02A	Bulk rock	18	41	90	12	20	4.7	2.6	9.9	5.6
SP12-02A	Clinopyroxene	-	-	820	-	392	-	-	-	-
SP12-02A	Orthopyroxene	-	-	184	-	174	-	-	-	-
SP12-02C	Bulk rock	16	27	70	11	20	4.0	2.5	8.5	5.0
SP12-02C	Clinopyroxene	-	-	802	-	301	-	-	-	-
SP12-02D	Bulk rock	21	33	90	12	20	4.3	2.5	9.4	5.3
SP12-02D	Clinopyroxene	24	0.7	946	-	725	7.4	<0.01	0.06	7.2
SP12-02D	Orthopyroxene	16	0.6	245	-	185	0.7	<0.01	<0.01	0.4
SP12-02E	Bulk rock	20	32	80	11	20	4.1	2.4	9.1	5.3
SP12-02E	Clinopyroxene	-	-	410	-	384	-	-	-	-
SP12-02F	Bulk rock	18	42	70	11	20	4.2	2.2	8.3	5.2
SP12-02F	Clinopyroxene	-	-	366	-	142	-	-	-	-
SP12-02F	Orthopyroxene	-	-	109	-	171	-	-	-	-

Major and trace elements in lava (bulk rock) were measured by ICP-OES and ICP-MS, respectively, in aliquots of ca. 1 g.
Major element concentrations in phenocrysts represent mean values that were determined by electron-microprobe on 10-15 grains per sample. Absolute standard deviations associated with mean values are <1% in mass (1σ).
MnO and P2O5 analyses in phenocrysts were substituted by NiO and Cr2O3 (values are shown as traces and represent <0.2 % in mass of the total pyroxene composition)
Trace element concentrations in phenocrysts represent mean values that were determined by Laser ICP-MS on ca. 15 grains per samples. Relative standard deviations (1σ) represent ca. <15% (Li), 40% (B, Gd and Sm) and >50% (U and Th).

Table 4. Summary of the SP12-02A ^{40}Ar-^{39} step heating experiment.

Incremental heating	$^{40}Ar/^{39}Ar$	$^{37}Ar/^{39}Ar$	$^{36}Ar/^{39}Ar$	^{40}Ar (%)	K/Ca	^{39}Ar (%)	Age ± 1σ (ka)
#1	0.1547	0.1727	0.0381	1.36	2.49	9.87	98.9±24.9
#2	0.1708	0.1384	0.0587	0.98	3.11	19.14	109.2±39.8
#3	0.1476	0.2527	0.0507	0.98	1.70	7.50	94.3±35.6
#4	0.1805	0.1416	0.0407	1.48	3.04	22.30	115.4±23.8
#5	0.1873	0.3236	0.0529	1.18	1.33	10.31	119.8±40.1
#6	0.1765	0.2447	0.0580	1.02	1.76	14.77	112.8±37.5
#7	0.1752	0.4887	0.0904	0.65	0.88	5.70	112.0±73.5
#8	0.1587	0.3469	0.0509	1.04	1.24	10.40	101.5±30.3
Total fusion	0.1712	0.2275	0.1042		1.89		109.4±13.2
Plateau	0.1674				1.40		107.0±11.6

Table 5. Helium analyses

Sample Name	Mineral	Mass	^3He_t	^4He_t	$P3_n$	^3He_n	$P4_r$	^3He_c	$^3He_{c(S)}$	P^3He_c
		(mg)	(Mat.g^{-1}) [a]	(10^3 Mat.g^{-1}) [a]	(at.g^{-1}.yr^{-1}) [b]	(Mat.g^{-1}) [c]	(Mat.g^{-1}.yr^{-1}) [d]	(Mat.g^{-1}) [e]	(Mat.g^{-1})	(at.g^{-1}.yr^{-1}) [f]
SP12-02A	Clinop.	22.9	96.0±2.6	89.9±15.7	0.2	0.02	1.19	95.7±2.6	100.7±2.7	941±25 (105)
SP12-02A	Orthop.	12.2	96.6±3.3	29.9±29.5	0.1	0.01	1.16	96.3±3.3	101.3±3.4	946±32 (108)
SP12-02A	*Average*	-	-	-	-	-	-	*95.9±2.0*	*100.9±2.1*	*943±20 (104)*
SP12-02C	Clinop.	27.8	91.9±2.4	71.6±13.0	0.2	0.02	1.12	91.6±2.4	*96.1±2.5*	898±23 (100)
SP12-02D	Clinop.	18.1	95.7±2.8	35.6±20.6	0.2	0.02	1.17	95.4±2.8	99.9±2.9	934±27 (105)
SP12-02D	Orthop.	16.4	89.2±2.8	76.9±22.8	0.1	0.01	1.11	88.9±2.8	93.0±2.9	870±27 (98)
SP12-02D	*Average*	-	-	-	-	-	-	*92.2±3.3*	*96.5±3.4*	*902±32 (103)*
SP12-02E	Clinop.	25.9	93.5±2.4	29.2±14.4	0.2	0.02	1.13	93.2±2.5	*98.0±2.6*	916±24 (102)
SP12-02F	Clinop.	25.9	93.0±2.3	29.2±14.4	0.1	0.02	1.04	92.7±2.3	101.5±2.6	949±24 (106)
SP12-02F	Orthop.	23.4	92.6±2.4	37.1±15.4	0.1	0.01	0.98	92.3±2.4	101.1±2.6	945±25 (106)
SP12-02F	*Average*	-	-	-	-	-	-	*92.5±1.7*	*101.3±1.8*	*947±17 (104)*

[a] ^{3}He and 4He concentrations measured by fusing the sample and corrected for blanks. Typical ^{3}He and ^{4}He blanks during the measurements were (3.3±1.1) × 10^4 atoms and (1.8±0.4) × 10^9 atoms, respectively, or <3% of ^{3}He and ca. 50-80% of ^{4}He measured in the samples. Associated errors (1σ) include sample and blank counting statistics as well as the one-sigma reproducibility on standard analyses over a 2 months period (1.5% for 3He and 0.3% for 4He).

[b] Nucleogenic ^{3}He production rates were calculated according to Andrews (1985) and Andrews and Kay (1982) using Li concentration measured in pyroxene aliquots and major and trace element compositions of lava (Table 2).

[c] Total nucleogenic ^{3}He calculated as the product of $P3_n$ and the age of the lava based on the Ar/Ar dating.

[d] Radiogenic ^{4}He production rate were predicted from equations described in Farley et al. (2006) and Blard and Farley (2008). Calculations are based on U, Th and Sm concentrations measured both in bulk rocks and clinopyroxene and orthopyroxene aliquots of sample SP12-02D (see Table 3) together with a measured equivalent spherical radius of 215 µm for pyroxene grains and an estimated 20-µm alpha-nuclei stopping distance.

[e] Corrected for magmatic (^3He_m) and nucleogenic (^3He_n) contributions to ^3He_T. The magmatic contribution was inferred from a 6 min in-vacuo crushing of an aliquot of sample SP12-02D that yielded concentrations of (0.29±0.09) Mat.g^{-1} and (17.0±0.6) × 10^3 Mat.g^{-1} for ^{3}He

and ^{4}He, respectively, which represented a $^{3}He/^{4}He$ isotopic ratio of 12±4 Ra. Reported errors (1σ) integrate ca. 3% uncertainty on $^{3}He_{t}$ measurements and 10% and 31% uncertainties on nucleogenic and magmatic contribution estimates, respectively.

[f] Local cosmogenic ^{3}He production rates estimated from $^{3}He_{c}$ concentrations scaled to the surface, an open-sky topography and 21.934°S-68.510°W and 3390 m a.s.l. and the age of the lava based on the $^{40}Ar/^{39}Ar$ dating. Bracketed values correspond to external errors (1σ) and include the ca. 3% uncertainty on $^{3}He_{c}$ concentrations and 11% on the $^{40}Ar/^{39}Ar$ inferred age of the lava.

Table 6. SLHL ^{3}He production rates from the San Pedro calibration site

Scaling scheme [a]	Atmosphere model [b]	Geomagnetic reconstruction [c]	SLHL P3 ($at.g^{-1}.yr^{-1}$) [d]
"St"	Standard	-	132±14
	ERA-40 (1)	-	143±16
"Lm"	Standard	Musheler-SINT2000	120±13
		GLOPIS75-SINT2000	118±13
		LSD	109±12
	ERA-40	Musheler-SINT2000 (2)	130±14
		GLOPIS75-SINT2000 (3)	128±14
		LSD (4)	118±14
"LSD"	Standard	Musheler-SINT2000	116±13
		GLOPIS75-SINT2000	113±12
		LSD	103±11
	ERA-40	Musheler-SINT2000 (5)	127±14
		GLOPIS75-SINT2000 (6)	124±14
		LSD (7)	112±12

[a] Cosmogenic ^{3}He production rates are scaled to the reference sea level high latitude (SLHL) position using the calculation procedures and employed the scaling frameworks reported by Martin et al. (2015). "St" refers to Lal (1991) / Stone (2000), "Lm" to the time-dependent adaptation of the Lal/Stone scheme (see e.g. Balco et al., 2008) and "LSD" to Lifton et al. (2014).

[b] The Standard atmosphere model is based on the National Oceanic and Atmospheric Administration (1976) and the ERA-40 reanalysis dataset on Uppala et al., (2005).

[c] Geomagnetic models rely on Virtual Dipole Moment values based on Muscheler et al. (2005), GLOPIS-75 (Laj et al., 2004) and SINT-2000 (Valet et al., 2005). Numbers in brackets refer to scaling factor curves as labeled in Figure 5.

[d] SLHL P3 estimates are obtained by dividing the local production rate by a scaling factor inferred for a given combination of scaling, atmosphere and geomagnetic reconstruction models (see text for details). Reported errors correspond to external (total) uncertainties at 1σ-level and comprise a ca. 1% uncertainty associated with the weighted average cosmogenic ^{3}He concentration and ca. 11% from the $^{40}Ar/^{39}Ar$ dating.

Figure captions

Figure 1. Geological sketch of the San Pedro volcano showing the location of the sampling site. The map is modified after Francis et al. (1974) and O'Callaghan and Francis (1986). Hillshade model and 100-m-interval contours are based on the ASTER GDEM 30-m-resolution digital topography. False easting and northing kilometer coordinates are based on UTM zone 19S projection. Inset shows the location of the San Pedro volcano in the Central Andes, the Atacama Desert as well as the Cerro Tunupa calibration site from Blard et al. (2013a).

Figure 2. Photograph collection of the sampling site. (A) General overview of the San Pedro volcano photographed from the SW lava flow at ca. 3600 m a.s.l. toward the NE. (B) Satellite image (Google Earth) showing the situation of samples (see red star in Figure 1). Note the lobate morphology of the lava front and the stream-oriented elongated features that correspond to crease structures. For representation purposes sample labels are shortened but should be read SP12-02(letter). (C) Picture taken from the sampling site (see position of SP12-02A) looking East toward the apex of the lava; a large crease structure can be seen in the background (see close up in D). Note that the sampled surface is perfectly smooth though fractured in m-scale compartments and displays stream-parallel striations that are characteristics of pristine crease-structures surfaces. (D) Close-up of the surface sampled for SP12-02A showing ~5-cm wide and few-mm high striations marked on top of the ca. 2-cm-thick rind. (E) Left half-part of the large crease structure situated at the apex of the sampled lava flow showing the general smooth and convex morphology of the rock wall as well as the subhorizontal striations and subvertical wall offsets characteristics of these features. Note the person (for scale) is located in the central valley of the crease structure. The materials forming this structure were exhumed from the central valley up. The second half of this structure can be seen on the right of the person.

Figure 3. $^{40}Ar/^{39}Ar$ ages obtained plotted vs. the cumulated amount of ^{39}Ar released for SP12-02A. The calculated plateau ages (ka±1σ) is presented with the MSWD value (n=8).

Figure 4. Camel diagram showing the distribution of cosmogenic ^{3}He concentrations obtained for the San Pedro volcano samples. ^{3}He concentrations are corrected for magmatic and nucleogenic contributions, scaled for geomorphic shielding and sample thickness and normalized to 21.934°S-68.510°W and 3390 m. Note that normalizing each sample's concentration to the surface, an open-sky topography and to a common coordinate allow to better identifying any potential outliers due to erosion or inheritance. Each individual cosmogenic ^{3}He concentration is represented as a Gaussian distribution, considering the concentration value and its 1σ-error. Green and dashed-brown curves represent clinopyroxene (n=5) and orthopyroxene (n=3) aliquots, respectively. Black curve represents the sum of individual curves. The weighted average concentration is calculated after averaging clino- and orthopyroxene values and is reported with its associated MSWD value.

Figure 5. (A) 150-ka-long variations of TCN scaling-factors and magnetic-field cutoff rigidity calculated for 21.934°S-68.510°W-3390 m a.s.l. using calculation procedures and scaling frameworks reported by Martin et al. (2015). All scaling factors are calculated based on the atmospheric pressure derived from the ERA-40 reanalysis dataset (Uppala et al., 2005). Numbers in brackets are the same as in Table 6 and represent predictions from different combinations of scaling schemes and geomagnetic field reconstructions. (B) Time-integrated scaling factors using the "Lm" scaling scheme and the ERA-40 atmosphere model with geomagnetic field reconstructions based on Musheler-SINT2000 (black curve) and as implemented in the "LSD" model (green curve). The red curves represent the production ratio between "Lm-LSD" and "Lm-Muscheler".

Figure 6. Distribution of the reevaluated SLHL P3s inferred from the compilation of previous geological calibration sites as well as the San Pedro lava flow. Values represented are inferred from the combination of the "Lm" scaling scheme with the ERA-40 atmosphere model and the geomagnetic field reconstruction relying on the VDM values based on Muscheler et al. (2005) for the period 0-62 ka and SINT2000 (Valet et al., 2005) beyond. (A) Camel diagram showing the distribution of reevaluated SLHL P3s. Inset illustrates the impact of the radiogenic correction applied on cosmogenic ^{3}He concentrations following Blard and Farley (2008) (see text). (B), (C) and (D) show the distribution of SLHL P3s as a function of latitude, elevation and calibration age, respectively. Note the absence of statistically significant relationships between the production rate and these parameters. Red data represents the San Pedro volcano calibration site.

Figure 1

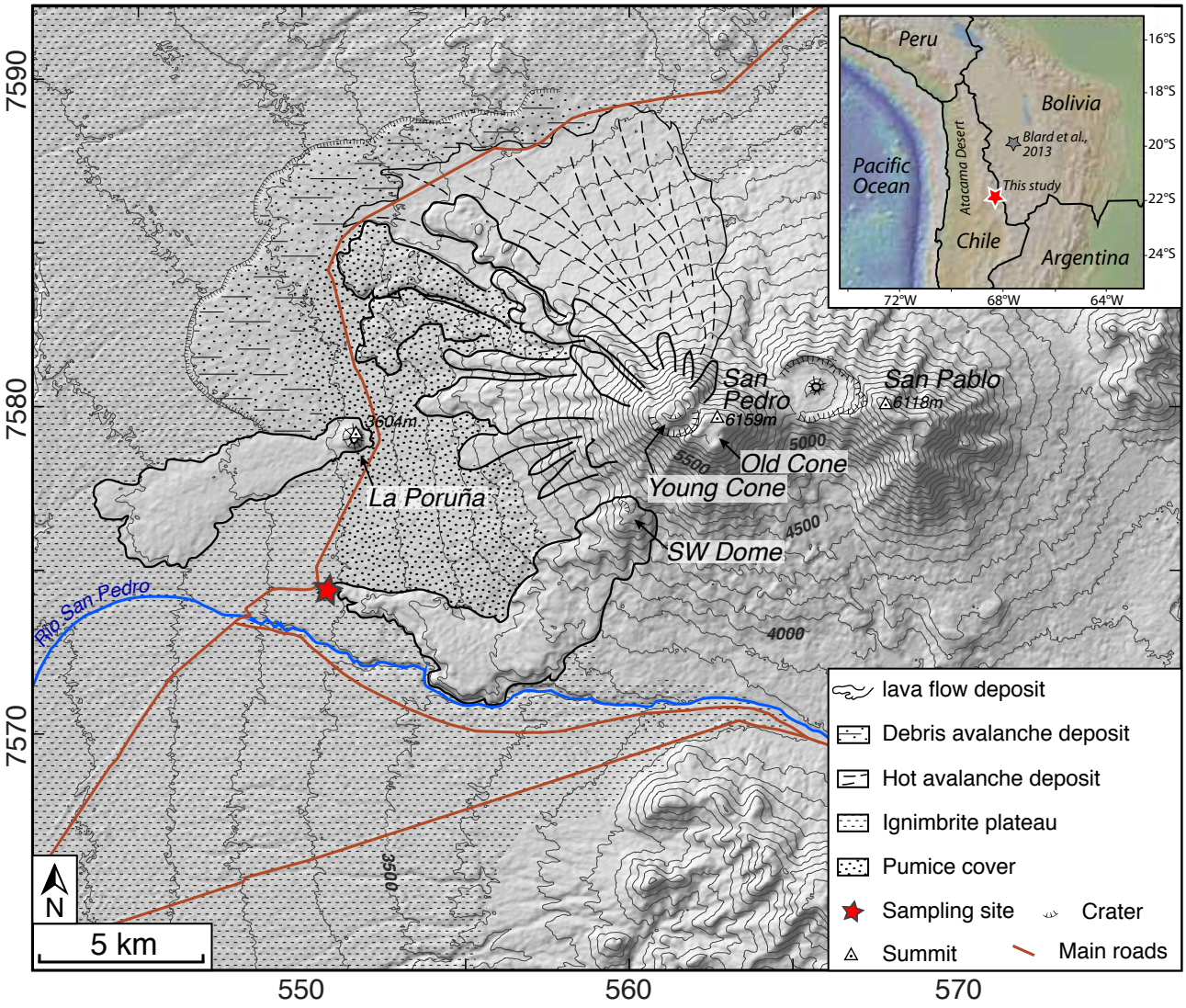
7590
7580
7570
550
560
570
San Pedro
6159m
San Pablo
6118m
3604m
La Poruña
Old Cone
Young Cone
SW Dome
5000
5500
4500
4000
3500
Río San Pedro
N
5 km
Peru
Bolivia
Pacific Ocean
Atacama Desert
Chile
Argentina
Blard et al., 2013
This study
16°S
18°S
20°S
22°S
24°S
72°W
68°W
64°W
lava flow deposit
Debris avalanche deposit
Hot avalanche deposit
Ignimbrite plateau
Pumice cover
Sampling site
Crater
Summit
Main roads

Figure 2

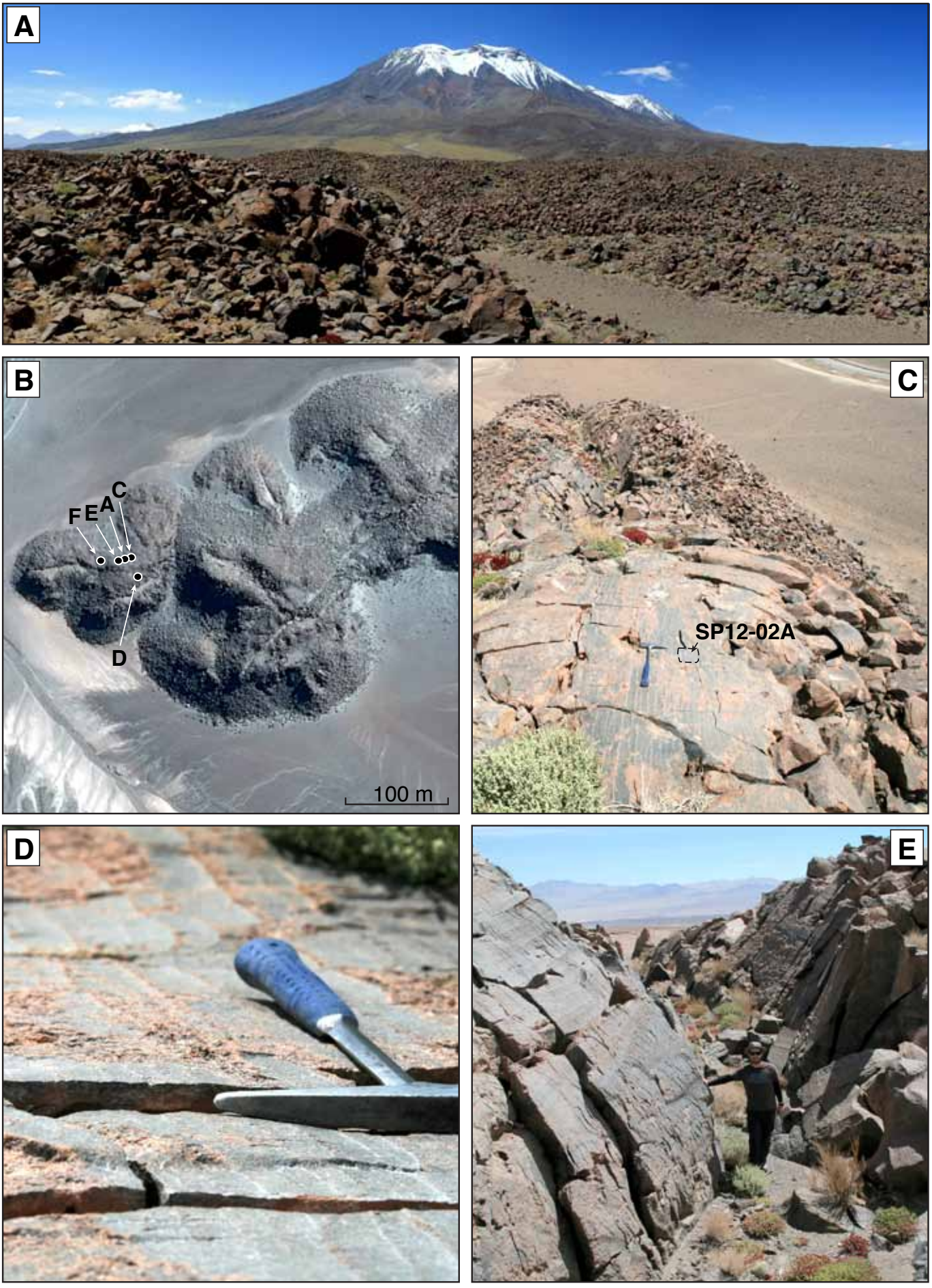

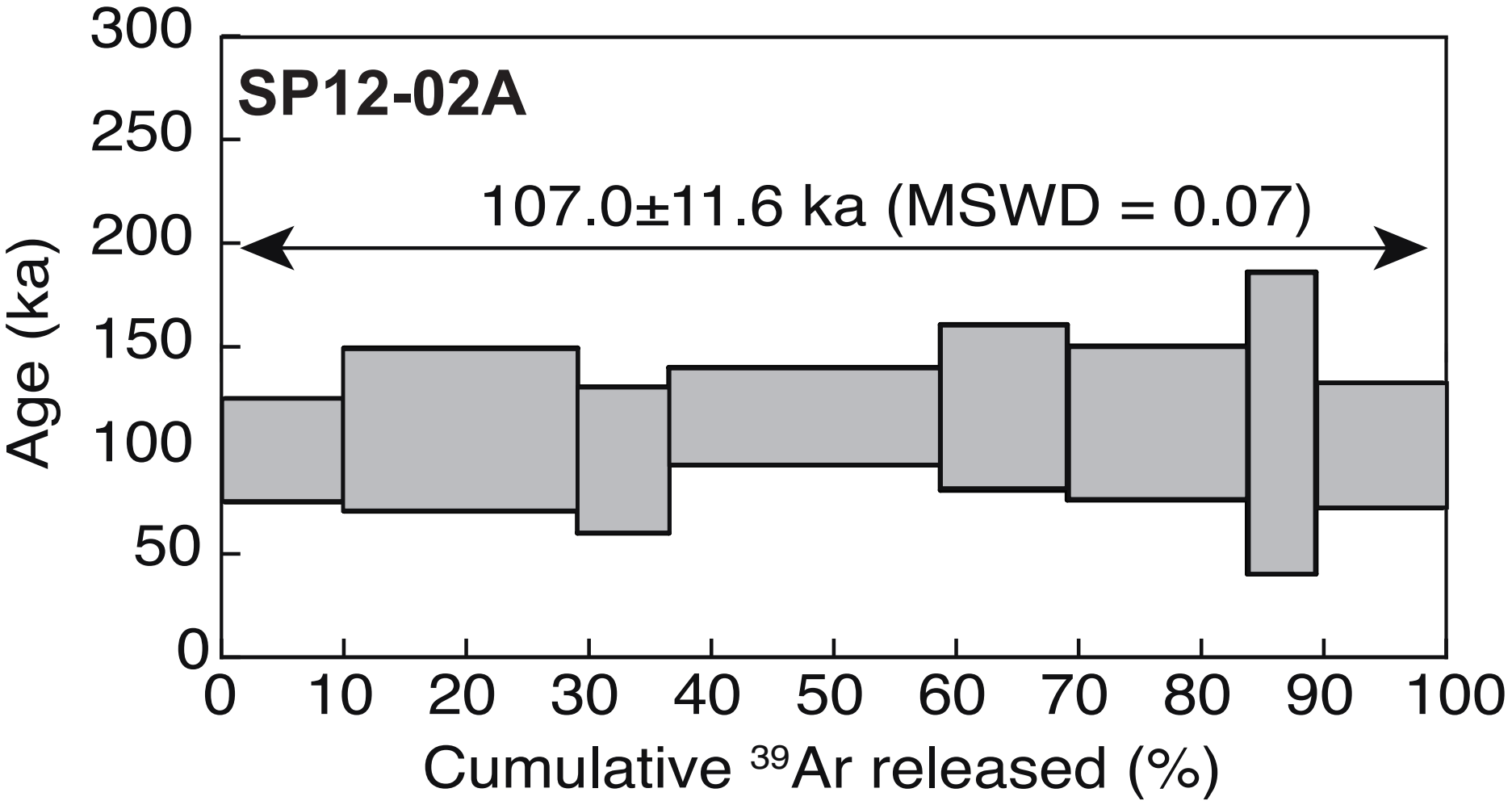
SP12-02A
107.0±11.6 ka (MSWD = 0.07)
Age (ka)
300
250
200
150
100
50
0
0
10
20
30
40
50
60
70
80
90
100
Cumulative 39Ar released (%)

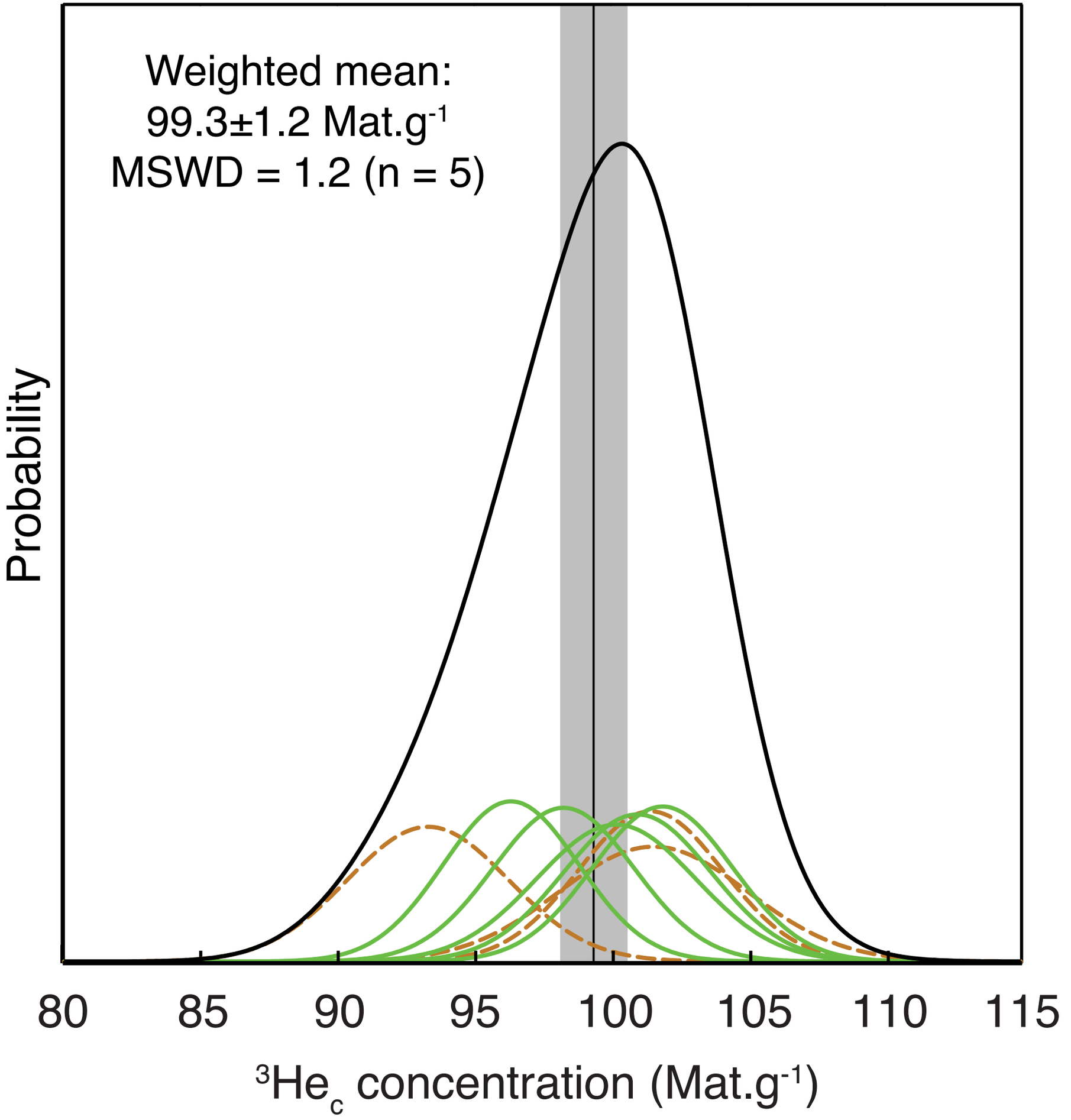
Weighted mean:
99.3±1.2 Mat.g-1
MSWD = 1.2 (n = 5)
Probability
80
85
90
95
100
105
110
115
3He c concentration (Mat.g-1)

Figure 5

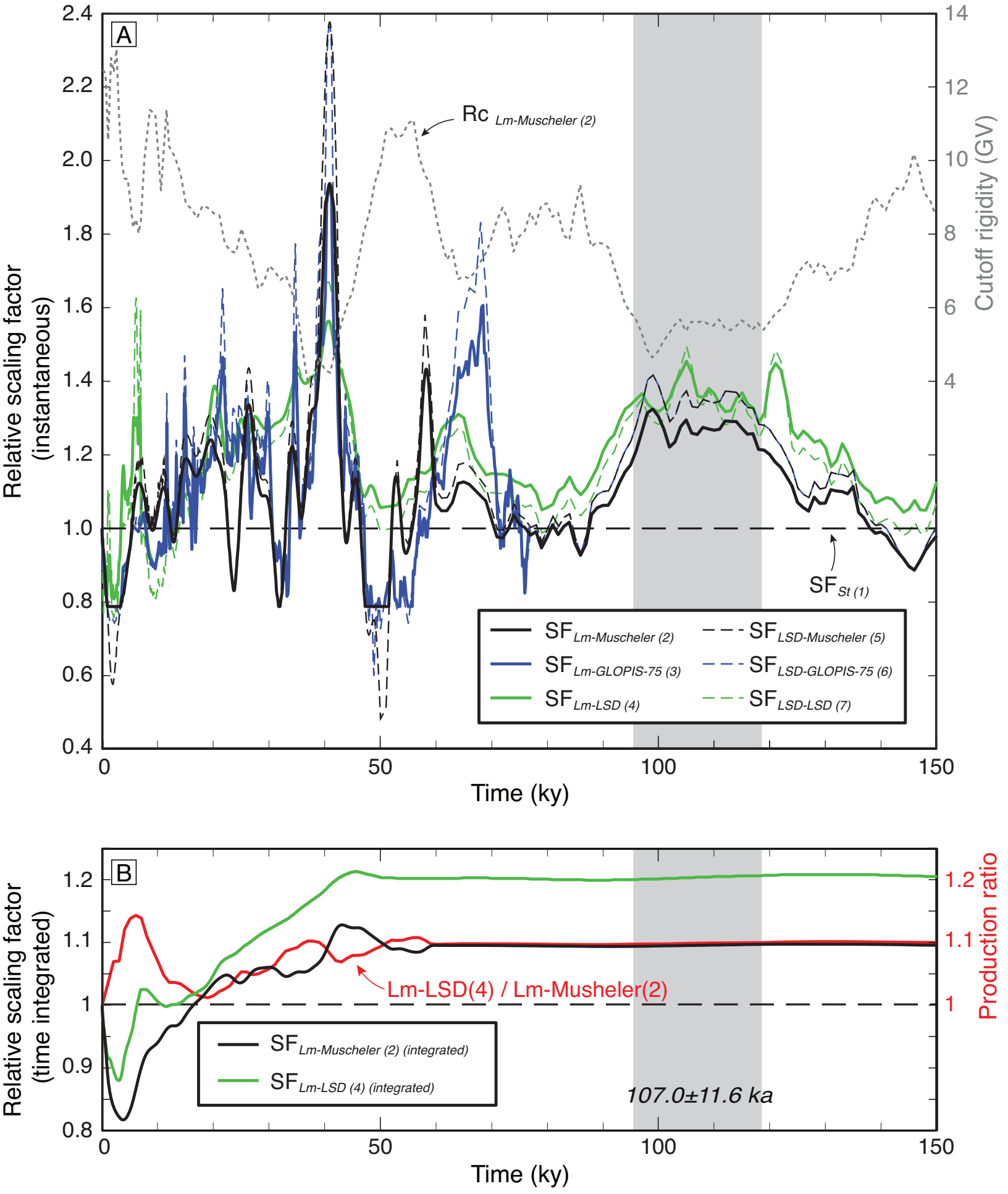
A
Rc Lm-Muscheler (2)
Relative scaling factor (instantaneous)
Cutoff rigidity (GV)
SF St (1)
SF Lm-Muscheler (2)
SF Lm-GLOPIS-75 (3)
SF Lm-LSD (4)
SF LSD-Muscheler (5)
SF LSD-GLOPIS-75 (6)
SF LSD-LSD (7)
Time (ky)
B
Relative scaling factor (time integrated)
Production ratio
Lm-LSD(4) / Lm-Musheler(2)
SF Lm-Muscheler (2) (integrated)
SF Lm-LSD (4) (integrated)
107.0±11.6 ka
Time (ky)

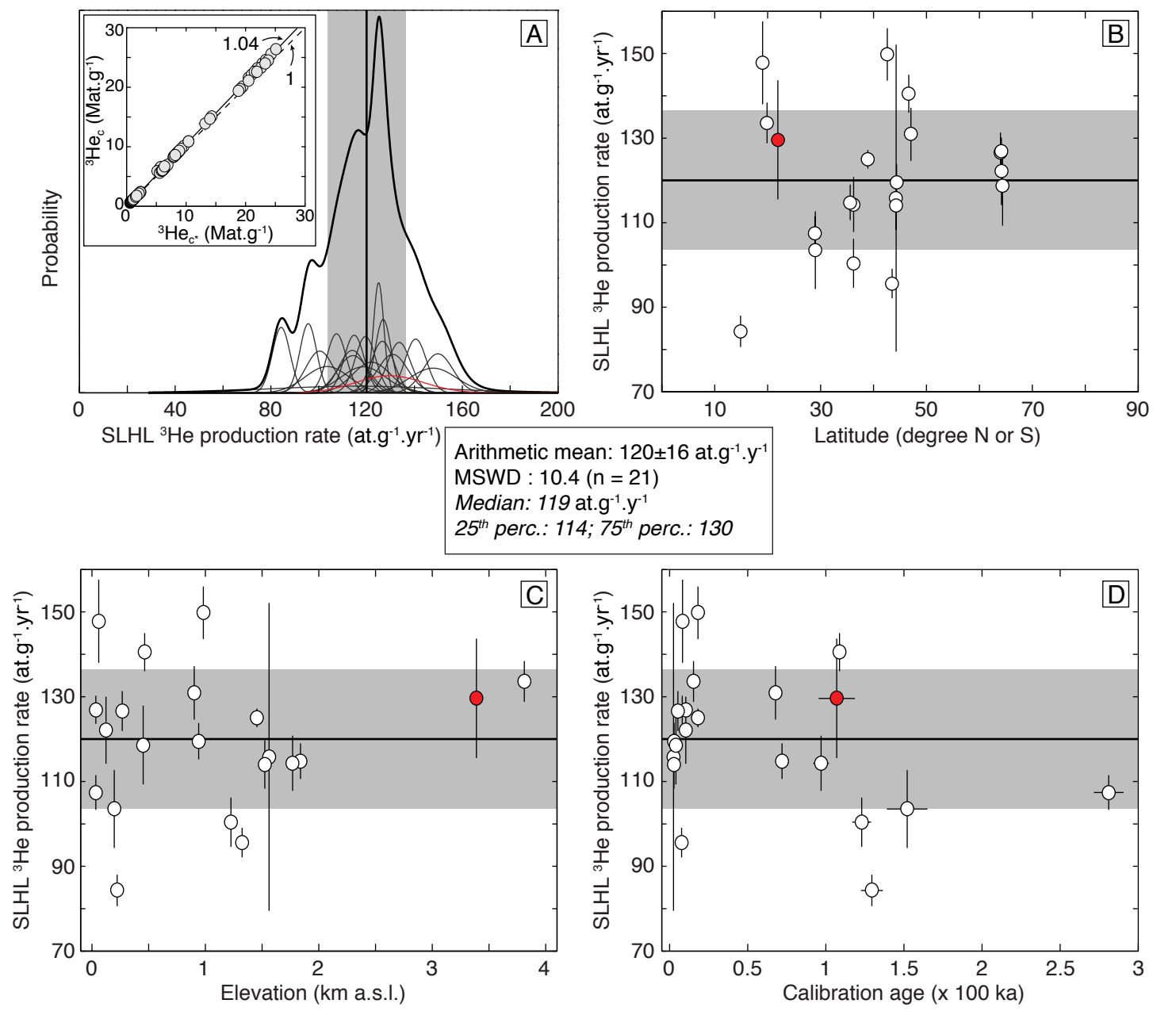
A
B
C
D
Probability
SLHL ^{3}He production rate (at.g^{-1}.yr^{-1})
^{3}He$_c$ (Mat.g^{-1})
^{3}He$_{c^*}$ (Mat.g^{-1})
1.04
1
Arithmetic mean: 120±16 at.g^{-1}.y^{-1}
MSWD : 10.4 (n = 21)
Median: 119 at.g^{-1}.y^{-1}
25th perc.: 114; 75th perc.: 130
Latitude (degree N or S)
Elevation (km a.s.l.)
Calibration age (x 100 ka)